TILDA-V: A full-differential Monte Carlo track structure for proton transport modeling in biological matter

SAND2016-0496J

M. A. Quinto[1], J. M. Monti[1], P. F. Weck[2], O. A. Fojón[1], J. Hanssen[1], R. D. Rivarola[1], P. Senot[3] and C. Champion[4,†]

[1]Instituto de Física Rosario, CONICET, Universidad Nacional de Rosario, Rosario, Argentina

[2]Sandia National Laboratories, Albuquerque, NM, USA

[3]Université de Lorraine, CNRS, Institut de Chimie, Physique et Matériaux, Metz, France

[4]Université de Bordeaux, CNRS/IN2P3, Centre d'Etudes Nucléaires de Bordeaux Gradignan, CENBG, Gradignan, France

Abstract

Understanding the radiation-induced effects at the cellular level is of prime importance for predicting the fate of irradiated biological organisms. Thus, whether it is in radiobiology to identify the DNA critical lesions or in medicine to adapt the radio-therapeutic protocols, an accurate knowledge of the numerous interactions induced by charged particles in living matter is required. Monte-Carlo track-structure simulations represent the most suitable and powerful tools, in particular for modelling the full slowing-down of the ionizing particles in biological matter. However most of the existing codes are based on semi-empirical cross sections as well as the use of water as surrogate of the biological matter. The current work aims at going beyond this artifice with the development of an *event-by-event* Monte Carlo code **-** called *TILDA-V* (a French acronym for Transport d'Ions Lourds Dans l'Aqua & Vivo) - based on a complete set of *multiple differential* and *total* cross sections for describing all the inelastic and elastic processes occurring throughout the slowing-down of 10keV-100MeV protons in both water and DNA.

Keywords: Monte Carlo, proton transport, water and DNA, CDW-EIS.

[†]Corresponding author:

Prof. Christophe Champion

Centre d'Etudes Nucléaires de Bordeaux Gradignan, Chemin du solarium, 33170 Gradignan

CENBG/CNRS/ IN2P3/Université de Bordeaux

Tel: +33 (0)5-57-12-08-96

E-mail: champion@cenbg.in2p3.fr

Introduction

Phenomena associated with radiation action in matter include a wide variety of physical, chemical and biological processes. It is nowadays well accepted that the nature of these interactions depends both on the type of radiation and on the impact energy. Thus, whether it is in radiobiology to identify the DNA critical lesions or in medicine to adapt the radio-therapeutic protocols, a fine understanding of the radio-induced interactions in living matter is required. Numerical simulations such as the well-known Monte Carlo (MC) approach represent the most suitable and powerful tools, with a large spectrum of applications in various fields including nuclear physics, astrophysics, plasma physics, solid state physics, accelerator driven systems, radioprotection, radiobiology and medicine (radiotherapy and nuclear imaging).

Among the existing MC codes (see the review given by Nikjoo *et al* 2006 and the brief summary reported in Table 1), some of them - known as condensed-history codes - are based on a macroscopic description of the particle transport (multiple scattering theory) and mainly developed for general-purpose applications. In this context, let us cite Geant4 (Agostinelli *et al* 2005), PHITS (Iwase *et al* 2002), FLUKA (Fasso *et al* 2005), MCNPX (Hendricks *et al* 2005), EGS (Nelson *et al* 1985), which are used in high-energy physics, detector simulation, space radiation and medicine. However, in the ambit of micro-dosimetry, these MC codes appear as limited and not able to predict the radio-induced energy deposits at the *nanometric* level and are therefore generally supplanted by MC *track-structure* (MCTS) approaches where the full particle histories are described step-by-step, interaction after interaction for both the incident beam and the secondary particles potentially created. It is worth noting that the development of such event-by-event MCTS codes has been rather slower than the condensed-history codes, since it requires the building-up of a large set of input data (cross sections) essential to describe at the atomic scale the various particle-induced interactions in the medium of interest (water and DNA). Besides, some existing codes extend their scope to the simulation of the DNA damage induction by modeling the ensuing chemical stage (see for example Gervais *et al* 2005, Plante 2011, Friedland *et al* 2011) and by considering specific DNA structure models (Friedland *et al* 1998, 2011, Bernal *et al* 2013, 2015).

Generally speaking, all the MCTS codes devoted to modeling charged particle tracks in biological matter (ions, electrons and positrons) include input databases taken from different standards (see for example ICRU, IAEA), mainly based on experimental data or semi-empirical approaches. Drawing up an exhaustive list of models implemented into the MCTS codes documented in the literature would be a daunting task in view of the variety of existing approaches and we refer the interested reader to the dedicated references listed in Table 1. Nevertheless, from a general standpoint, it is worth noting that the predictive power of such models remains either restricted to the domain of validity of the theoretical approximations used or limited by the availability of experimental data. Regarding the latter, we essentially find in the literature total cross sections, the multiple differential cross sections - needed to describe the angular and the energetic distributions of the secondary emitted electrons - being indeed rarely investigated due to the complexity of simultaneous energetic and angular detection. Therefore, semi-empirical laws are usually preferred in the

transport numerical simulations, although the paucity of measured data may sometimes lead to questionable results largely based on extrapolations.

Location of Table 1

Table 1. Monte Carlo codes available in the literature

Considering first the proton-induced ionization in water, examination of the literature dedicated to MCTS codes reveals that two main models have been used. The first one, hereafter denoted Rudd's model (Rudd 1989) was initially developed for protons impacting atomic and molecular targets. It provides an analytic equation for the energy distribution of electrons by means of a large set of fitting parameters deduced from experimental comparisons. It is based on a simple version of the binary-encounter approximation equation modified to yield the correct high-energy asymptotic dependence on energy in agreement with the Bethe equation prediction and further modified by the use of the promotion model at low energies. In brief, the approximation made consists in treating the collision - between a projectile and a single target electron - as a classical one. The nucleus and the remaining target electrons play no role except to provide a binding energy for the ejected electron. The justification for using a classical model lies in the fact that doubly differential cross sections for Coulomb scattering between two particles are the same when calculated using either classical physics or quantum mechanics. The second semi-empirical and well-documented model - called HKS model since developed by Hansen, Kocbach and Stolterfoht (Hansen and Kocbach 1989) - consists in describing the ionization process within the impact parameter 1st Born approximation. In this approach, the initial and the final electron states are described by means of a hydrogenic function and a plane wave, respectively, i.e. without taking into account the electron momentum in its bound state. However, due to singularities observed when the ejected electron energy tends to zero, further empirical fittings were employed to finally provide the well-known HKS model.

When the proton energy becomes sufficiently low (< 100 keV/u), the ionization probability diminishes rapidly and the capture process becomes the predominant energy-loss pathway. However, only rare experimental measurements have been reported so far for water. To overcome this lack, many semi-empirical simulations have been proposed for modeling the electron capture process. Let us cite the approach proposed by Rudd *et al* (1983), which consists in expressing the charge transfer cross section σ as $\sigma = \sigma^+ - \sigma^-$ by means of adjustable parameters for fitting the measured cross sections of positive (ion) and negative (electron) charge production (σ^+ and σ^-, respectively). The resulting cross sections agree well with the experimental data for proton energies ranging in 1-100 keV, but exhibit large discrepancies with the experimental measurements (Lindsay *et al* 1997, Dagnac *et al* 1970 and Toburen *et al* 1968). More recently, Dingfelder *et al* (2000) suggested to express the charge transfer cross sections by analytical formula (straight lines for low and high proton energies on a doubly logarithmic scale, both connected by a power law) where the parameters were chosen by considering available experimental data.

In this context, we recently developed a series of theoretical models to estimate the ionization as well as the electron capture cross sections for protons colliding with water molecules (Champion *et al* 2013, Rivarola *et al* 2013). These models - based on either the 1st Born approximation with correct boundary conditions (CB1 model) or the continuum distorted wave-eikonal initial state approach (CDW-EIS model) - are detailed in the following. However, let us first here remind that the CB1 model describes the active (ejected) electron as being in bound and continuum states of the target field in the entry and exit channel, respectively, while in the CDW-EIS approximation, a more 'complete' representation of the active electron is introduced, considering that it evolves in the simultaneous presence of the projectile and target fields in the entry and exit channels at all collision times, for single ionization as well as for single electron capture. In this way, CB1 is a one-center model whereas CDW-EIS is a two-center one. Besides, let us add that correct boundary conditions are considered in the present CB1 model, meaning that asymptotic Coulomb long-range interactions between the projectile and all the particles composing the target are accounted for in the initial and final wave functions. Finally, let us remind that both present models are expected to be valid for high enough collision energies. Indeed, the CDW-EIS model has been introduced to give a better description than the one-center models of both the ionization and the capture processes, in particular in the intermediate impact energy regime *i.e*. where the impact velocity is comparable to the initial electron orbital velocity. Let us note that such quantum-mechanical models remain difficult to utilize, in particular for molecular targets, and are therefore rarely used in MCTS simulations. Nevertheless, some codes use CDW-EIS cross section databases, in particular for modeling the proton-induced ionization and capture processes: let us cite the work of Wiklund *et al* (2008) where light-ion beam secondary electron dose profiles in water were computed within the CDW-EIS framework and the recent LIonTrack code reported by Bäckström *et al* (2013) where the CDW-EIS formalism is used to generate the initial energy and angle of secondary electrons emitted in ionizing collisions of light ions with H_2O molecules.

Besides, it is worth mentioning that all these models were first developed for modeling the proton transport in water considered in its vapor phase. Lately, many groups have investigated the transport of charged particles in liquid water and then provided a theoretical approach of the proton-induced ionization processes (see for example Dingfelder *et al* 1998, 2000 and Garcia-Molina *et al* 2011). In almost all cases, the cross sections are calculated within the plane wave Born approximation by taking into account a phenomenological dielectric-response function model deduced from reflectance measurements - originally suggested by Ritchie and co-workers (Ritchie *et al* 1978, Hamm *et al* 1982, 1985) - for modeling the liquid environment (see for example the recent work of Dingfelder 2014 and the review provided by Emfietzoglou *et al* (2013)).

Modeling the full slowing-down of protons down to their neutralization in matter, namely, the Bragg peak region implies an accurate knowledge of *all* the inelastic interactions induced by the incident particle itself as well as its "derivatives". Thus, in addition to the two above-discussed proton-induced ionization and electron capture, a MCTS code needs to describe the neutral-hydrogen-induced ionization and electron-loss (stripping) processes. Unfortunately, these processes have been rarely investigated both theoretically and

experimentally. Thus, to overcome the lack of available experimental measurements and theoretical support, semi-empirical approaches - mainly based on simple scaling and fitting rules - were preferred (see for example Dingfelder *et al* 2000, Endo *et al* 2002). Similarly, the excitation process induced by both protons and neutral hydrogen atoms is commonly modeled by means of semi-empirical formulae (Dingfelder *et al* 2000, Endo *et al* 2002).

Providing a full description of the proton histories in biological matter implies tracking secondary electrons, which may be potentially generated along the proton and hydrogen tracks. To date, there are a number of Monte Carlo electron track-structure codes that have been developed independently to investigate the microscopic features of ionizing radiation in liquid and gaseous water (see Uehara *et al* 1999 and references therein). The existing codes use a variety of models and assumptions for treating the physical processes (elastic scattering, ionization and excitation channels), some of them being based on semi-empirical approaches whereas others were developed within a pure quantum mechanical framework (see for example the EPOTRAN code developed by Champion *et al* 2012a).

Finally, needless to say that the majority of existing numerical codes devoted to proton-induced damage modeling and its numerous derivatives (radiotherapy, dosimetry, medical imaging…) are based on the use of water as tissue-equivalent medium with – for the most sophisticated – the inclusion of the molecular DNA structure, which is finally superimposed on the ion track-structure in water (Friedland *et al* 1998). However, it is nowadays well known that the history of any charged particle in matter and, consequently, the energy deposit pattern are sensitive to the nature of the molecules impacted. Thus, in order to address such shortcomings, we recently proposed a series of quantum-mechanical models for describing the main ionizing processes induced by protons (see Champion *et al* 2010, Galassi *et al* 2012 and Champion *et al* 2012b for ionization and electron capture, respectively) and the electron-induced ionization (Champion 2013) in DNA.

In this context, the present work aims at going beyond this artifice, which consists in using water as surrogate of the biological medium, and at reporting on a newly developed track-structure code, called *TILDA-V* (Quinto *et al* 2015). *TILDA-V* (a French acronym for **T**ransport d'**I**ons **L**ourds **D**ans l'**A**qua & **V**ivo) refers to an extension of the *TILDA* Monte Carlo code previously developed by Champion *et al* (2005) for modeling heavy ion and secondary electron histories in liquid and gaseous water for impact energies ranging from 10 keV/u to 100 MeV/u. The current version is based on a complete set of quantum-mechanically calculated multiple differential and total cross sections for describing all the inelastic processes occurring throughout the slowing-down of protons in water and DNA components (adenine (A), thymine (T), cytosine (C), guanine (G) and sugar phosphate (SP) backbone).

To the best of our knowledge, *TILDA-V* represents the first Monte Carlo track-structure code able to simulate the full transport of protons and its secondaries in a "realistic" biological medium by means of *a complete set of quantum-mechanically based multiple-differential and total cross sections*. Comparisons with existing MCTS code predictions in terms of macroscopic observables (proton range, electronic stopping power, dose profiles…) are also provided. In all cases, we analyzed the influence of the various

theoretical models used for describing the proton-induced interactions and reported an intrinsic comparison between water and DNA.

1. The *TILDA-V* code

1.1. Charged particle transport

From a general point of view, charged particle transport simulation comprises series of sampling steps, which first determine the distance λ between two successive interactions. This latter is selected by assuming that the charged particle transport in matter is governed by a Poisson law $p(\lambda)$, whose corresponding probability $P(\lambda)$ is defined by

$$P(\lambda) = \int_0^{\lambda} p(u)du = 1 - \exp\left(\frac{-\lambda}{\bar{\lambda}}\right). \quad (1)$$

This probability is then randomly sampled by means of pseudo-random variables defined in the interval [0;1], namely, $\Gamma \equiv \Gamma(0;1)$, that finally leads to a distance λ given by

$$\lambda = -\bar{\lambda}\ln(1-\Gamma) = -\bar{\lambda}\ln(\Gamma') \text{ with } \Gamma' \equiv \Gamma'(0;1). \quad (2)$$

In Eq.(1), $\bar{\lambda}$ refers to the mean free path defined as $\bar{\lambda} = 1/(N\sigma_T)$ where N denotes the number of target molecules per volume unit defined as $N = N_A * \rho/A_{mol}$ where N_A is Avogadro's number, ρ and A_{mol} the density (in g.cm^{-3}) and the molar mass of the crossed medium, respectively, and σ_T the total cross section including all the interactions considered for modelling the transport of the particle of interest.

In its current version, *TILDA-V* takes into account the following collisional processes:

- ✓ for protons: elastic scattering, ionization, capture and excitation;
- ✓ for neutral-hydrogen atoms: elastic scattering, ionization, capture, electron loss (stripping) and excitation;
- ✓ for secondary electrons: elastic scattering, ionization and excitation.

Let us note that proton-induced multiple processes, such as double ionization and ionizing transfer, are not included yet. However, preliminary calculations performed within a classical trajectory Monte Carlo (CTMC) framework have demonstrated their relevance (Lekadir *et al* 2009a, 2009b) and quantum mechanical calculations actually in progress should be introduced into the next version of the code. Similarly, the double ionization process induced by electron impact in water recently studied by Oubaziz *et al* (2015) within the 1st Born approximation should be also accounted for in the near future.

The second sampling refers to the collision type occurring at the selected position. Whether it is for primary protons or secondary electrons, the latter is randomly chosen according to the relative magnitude of the individual total cross section of each collisional process (elastic as well as inelastic). The collision type *n* is simply given by

$$\sum_{i=1}^{n-1} P_i \leq \Gamma \leq \sum_{i=1}^{n} P_i \text{ with } P_i = \frac{\sigma_i}{\sigma_T}. \quad (3)$$

Then, if the selected interaction is ionizing, a third sampling procedure is performed in order to select the molecular subshell impacted. To do that, the procedure reported in Eq.(3) is once more followed by considering the contribution of each subshell to the total cross section of the selected process, namely, by using the *partial* cross sections. Besides, if excitation is selected, a similar procedure is followed for choosing the final excited state of the target, here again determined by the relative contribution of the *partial* cross sections.

Finally, in a last step, random samplings are performed in order to quantify the full kinematics of the selected interaction. This step is obviously the most time consuming step since it requires to access to the huge database needed for describing the numerous collisional processes. In fact, the latter includes:

- ✓ singly differential cross sections $\frac{d\sigma}{d\Omega_s}$ needed for describing the angular distribution of the *scattered* particle (electron, proton and hydrogen atom) during the elastic scattering process;
- ✓ singly and doubly differential cross sections $\frac{d\sigma}{\mathrm{d}E_\mathrm{e}}$ and $\frac{d^2\sigma}{d\Omega_e \mathrm{d}E_\mathrm{e}}$ needed for describing the energetic and the angular distributions of the ejected electron during the neutral-hydrogen-atom induced electron loss process;
- ✓ singly and doubly differential cross sections $\frac{d\sigma}{\mathrm{d}E_\mathrm{e}}$ and $\frac{d^2\sigma}{d\Omega_e \mathrm{d}E_\mathrm{e}}$ needed for describing the energetic and the angular distributions of the ejected electron during the proton and neutral-hydrogen-atom induced ionization process;
- ✓ singly, doubly and triply differential cross sections $\frac{d\sigma}{\mathrm{d}E_\mathrm{e}}$, $\frac{d^2\sigma}{d\Omega_e \mathrm{d}E_\mathrm{e}}$ and $\frac{d^3\sigma}{d\Omega_s d\Omega_e \mathrm{d}E_\mathrm{e}}$ needed for describing the energetic and angular distributions of the ejected and scattered electrons during the electron-induced ionization process (see Figure 1).

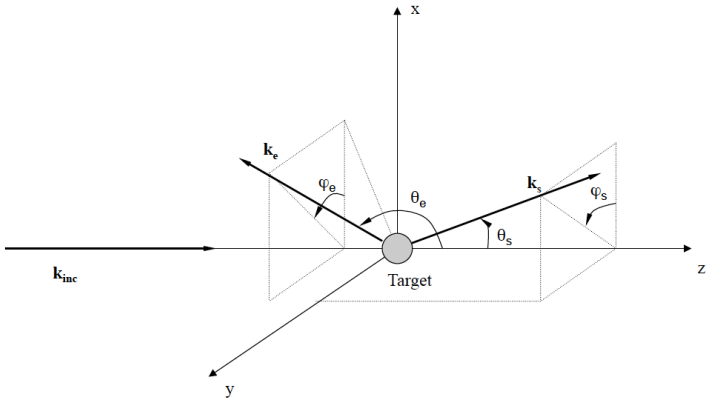

Figure 1. Reference frame of the electron-induced ionization process. $\boldsymbol{k_i}$, $\boldsymbol{k_s}$ and $\boldsymbol{k_e}$ represent the wave vectors of the incident, scattered and ejected electrons, respectively. The corresponding polar and azimuthal angles are denoted θ_s, φ_s, and θ_e, φ_e, respectively.

All these input data represent a large amount of information (> 10Gb memory size) and are pre-calculated for:

- 37 incident proton energies E_i ranging from 10 keV to 100 MeV within a logarithmic grid;

- 101 values of ejected electron energy E_e (for each incident energy) logarithmically ranging from a minimal value of 0.1 eV to a maximal value $E_e^{max} = 4\frac{m_0}{M_p}E_i$ where M_p and m_0 refer to the proton and the electron mass, respectively;

- 181 values of polar angles (θ_e, θ_s) ranging from 0 to 180° within a linear grid.

They are finally stored by way of tables in which kinematical parameters are put in correspondence to their respective differential cross sections. However, contrary to the majority of MCTS codes, which sample the requested physical quantities (angular and energetic transfers) via the inverse-transform method, *TILDA-V* uses a *uniform* procedure that returns more rapidly the requested quantity x via the relation $x = P^{-1}(\Gamma(0;1))$ where the cumulative probabilities $P(x)$ is defined by

$$P(\mathrm{x}) = \frac{\int_0^x p(x')\,dx'}{\int_0^{x_{max}} p(x')\,dx'} \text{ with } (0 \leq \mathrm{P}(x) \leq 1). \tag{4}$$

Figure 2 illustrates the random selection of the ejection angle from the doubly differential ionization cross sections (DDCS) in the case of water ionization by 1 MeV incident proton and for E_e = 750 eV.

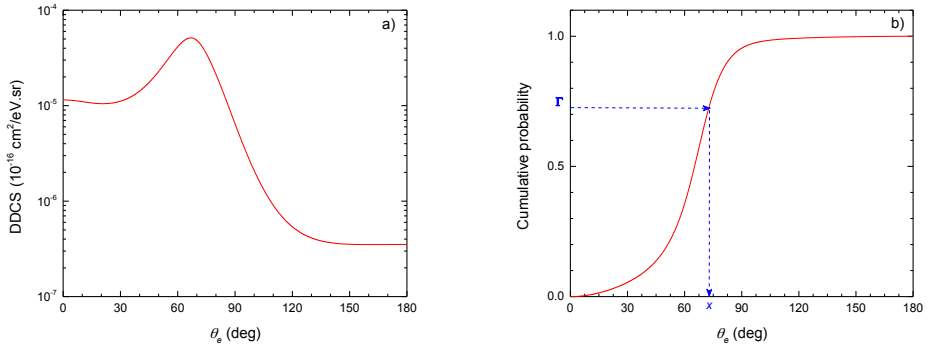

Figure 2. (Color online) a) Doubly differential ionization cross section plotted versus the ejection angle θ_e for 1 MeV incident proton ejecting a 750 eV electron from water (calculated within the *prior* CDW-EIS framework). b) Corresponding cumulative probability illustrating the random sampling procedure.

Once the collision type defined, the incident proton energy is reduced by the total energy transfer, which includes both the kinetic energy given to the secondary electron potentially created and the potential energy (binding energy, excitation energy,...) assumed as locally deposited. Besides, the charge state of the primary proton may also change according to the selected collision. Thus, the electron capture will decrease the initial proton charge (from +1 to 0) whereas the electron loss process (stripping) will increase the hydrogen charge (from 0 to +1). Note that the formation of H^- may also occur when the hydrogen atom captures an electron. However, due to the low magnitude of the hydrogen-induced capture cross section (see Abicht *et al* 2013), we have neglected this channel in the current version of *TILDA-V*.

Additionally, the full tracking of all the secondary electrons created along the various proton/hydrogen-induced collisions is completed by means of the above-cited set of multiple differential and total cross sections to characterize the ejection and scattering spectra along the electron-induced collisions.

All these steps are repeated for all primary and secondary particles until their kinetic energy falls below a predetermined cut-off value. For the primary particles, namely, protons and hydrogen atoms, the energy cut-off is fixed at 10 keV, while the secondary electrons are followed down to 7.4 eV, *i.e.* the excitation threshold of the water molecule. Secondary electrons with kinetic energies lower than this threshold are not followed and assumed as locally absorbed by the medium (see Figure 3).

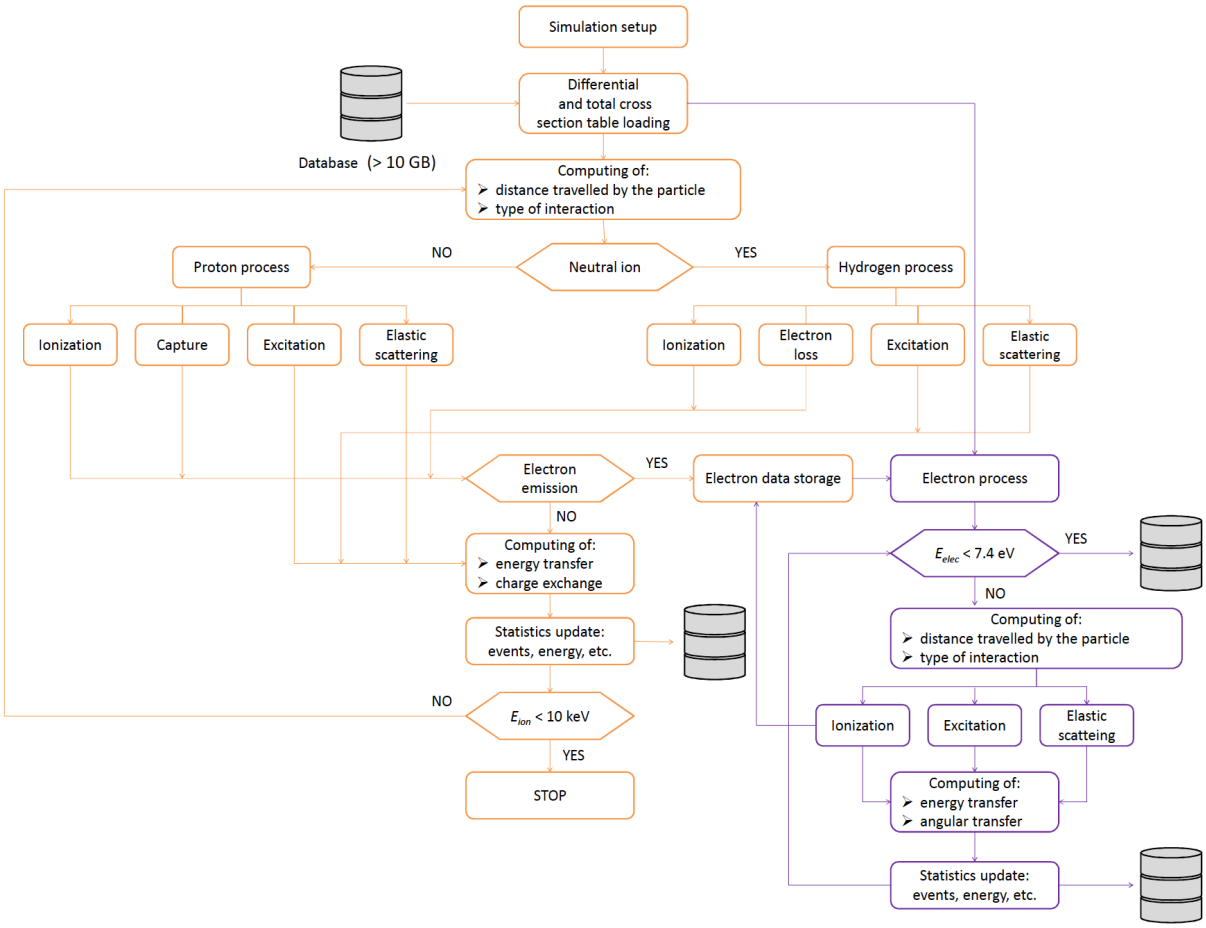

Figure 3. (Color online) Flow chart for primary proton and secondary electron transport in *TILDA-V*.

Besides, in the particular case of ionizing interactions of target inner-shells, it is well known that the vacancy may be accompanied by non-radiative transitions including the emission of Auger as well as Coster-Krönig electrons that takes place at a short time scale after the interaction, typically between 0.001 and 5 fs. These various processes have been considered in *TILDA-V* for all the targets investigated, namely, by considering the probability as well as the corresponding electron energy. For water, we used the data reported in Martin's thesis (2003), while for DNA we used the Auger electron non-radiative probabilities and energies provided by the Livermore Evaluate Atomic Data Library (Perkins and Cullen 1991) for the different atomic constituents involved in the biomolecular target description. All the data needed are reported in Table 2.

Location of Table 2

Table 2. Probabilities and corresponding energy transfers for the non-radiative transitions taken into account in *TILDA-V* for water and DNA.

1.2 Biological matter modeling: from water to DNA

Whether it is to describe the biological matter by water or via the main DNA components (A, C, T, G and SP), the biological medium has been modeled by means of molecular wave functions, all based on quantum mechanical calculations.

For water, we followed the SCF-LCAO (*self-consistent field - linear combination of atomic orbitals*) approach reported by Moccia (1964), who described the water molecule by means of single-center wave functions, all centered at a common origin (the oxygen atom). The latter refer to the equilibrium configurations calculated with the self-consistent field method and agree very well with the experimental geometrical and energetic properties of the water molecule. Regarding the DNA components, a single-center description of the targets is obviously less evident due to the multi-center nature of the molecules. In this context, we preferred an *ab initio* method in which all the molecular orbitals of each DNA component were described by a linear combination of atomic wave functions by using the GAUSSIAN09 software at the RHF/3-21G level (Frisch *et al* 2009). The equilibrium geometries of the nucleobases were then obtained without symmetry constraints applied, whereas the structure of the SP backbone unit was optimized following the procedure suggested by Colson *et al* (1993) for a typical B-DNA fiber conformation. The resulting first ionization potential of the backbone unit was 10.53 eV, in close agreement with the scaled value of 10.52 eV obtained by Bernhardt and Paretzke (2003), while the computed ionization energies of the occupied molecular orbitals of the nucleobases were scaled so that their calculated Koopmans ionization energy, *i.e.,* the ionization energy of their HOMO coincides with the experimental value of the ionization potential measured by Hush and Cheung (1975). Besides, the effective number of electrons relative to the atomic component was derived from a standard Mulliken population analysis. For more details, we refer the interested reader to our previous study (Galassi *et al* 2012) where all the quantum numbers and coefficients needed for expressing the target molecular wave functions are reported.

Furthermore, let us mention that the biomolecular targets under investigation in the current study are considered as *isolated* molecules and then refer to living matter components in *vapor* state. In this sense, the present work clearly differs from the existing studies on *condensed* matter (water or DNA) where the energy-loss function of realistic biological components was extracted from experimental data and interpolated for being used in cross section calculations [see for example the series of works provided by Abril and co-workers (Abril *et al* 2011, de Vera *et al* 2015) and that of Emfietzoglou *et al* (2003)].

Finally, in order to gain insight into the real energy deposit cartography induced by proton impact in biological medium, we have considered a typical nucleotide *i.e.* an equivalent unit of DNA molecule composed of a nucleobase-pair plus two SP groups (La Verne and Pimblott 1995). Additionally, to fit the realistic composition of living cells, we also took into consideration the nucleobase repartition percentages reported by Tan *et al* (2006), namely, 58% (A-T) (adenine-thymine base pair) and 42% (C-G) (cytosine-guanine base pair). Thus, by using the respective molar mass of each DNA component, namely, $M_A = 135.14$ g.mol^{-1}, $M_T = 126.12$ g.mol^{-1}, $M_C = 111.11$ g.mol^{-1}, $M_G = 151.14$ g.mol^{-1} and $M_{SP} = 180$ g.mol^{-1}, we obtained the following mass percentages: A (12.6%), T (11.8%), C (7.5%), G (10.2%) and SP group

(57.9%). However, this description refers to *dry* DNA, which obviously cannot intend to mimic the biological reality, mainly composed of hydrated DNA. Many studies have then shown that the mechanisms of degradation of DNA by direct energy deposition events were strongly dependent of the level of hydration of the nucleotide. Yokoya *et al* (2002) demonstrated that the yields of single-strand breaks (SSBs) and double-strand breaks (DSBs) slightly increased with respect to the level of hydration of DNA - from vacuum-dried DNA up to DNA containing 15 water molecules per nucleotide - the yields being constant at higher levels of hydration. The precise degree of hydration of macromolecules depends upon a variety of factors, including pH and concentration of salt in medium. Also, the value obtained varies with the method by which it is determined, some methods measuring only tightly bound molecules, while others also include water molecules more loosely associated with the macromolecule. Birnie *et al* (1973) estimated that the total amount of water associated with DNA was of the order of 50 moles per mole of nucleotide, in order to get the expected density of 1.29 g.cm^{-3}. Consequently, we also considered a biological medium composed of hydrated DNA here simulated by adding 18 molecules per nucleotide, that led to the following revisited mass percentages: A (8.3%), T (7.7%), C (4.9%), G (6.7%), SP group (38.1%) and water (34.3%). Thus, when particles cross hydrated DNA, a particular attention is given to the random samplings for precisely selecting the DNA component impacted and then the energy transfers that occurs. To do that, discrete values $x = 1, \ldots, 6$ were first attributed to the various nucleotide constituents ($x_{\mathrm{A}} = 1$, $x_{\mathrm{T}} = 2$, $x_{\mathrm{C}} = 3$; $x_{\mathrm{G}} = 4$, $x_{\mathrm{SP}} = 5$ and $x_{\mathrm{Water}} = 6$) with the corresponding interaction probabilities $p_1, \ldots, p_6$ that obviously include all the process cross sections (ionization, exchange charge and excitation). Then, by using the above-cited inverse-transform method, the impacted DNA component is chosen according to the relative probabilities, which also account for the nucleobase internal distribution, namely, 0.58 for adenine and thymine, 0.42 for cytosine and guanine, 2 for the sugar phosphate and 18 for the water). The method is depicted in Figure 4.

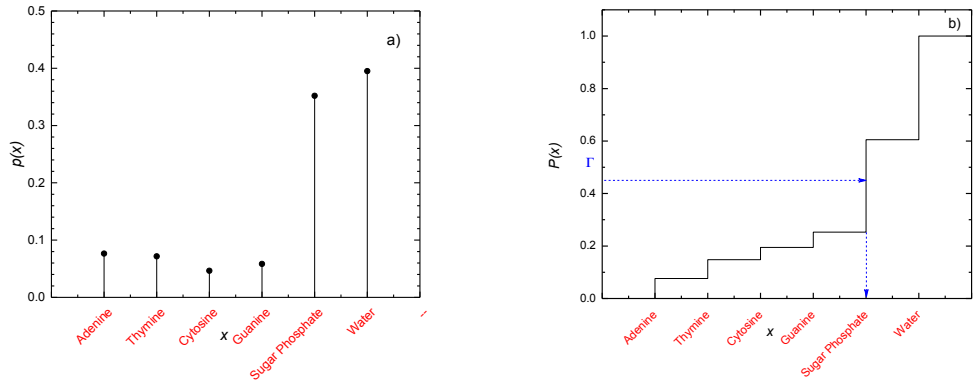

Figure 4. (Color online) a) Discrete probability function given by the sum of all the total interaction cross sections at a given incident proton energy for the various DNA components and water. b) Discrete probability density function sampled by the inverse-transform method (see Eq.(3)).

Additionally, in *TILDA-V* we used the cell geometry reported by Douglass *et al* (2012), where the main cellular structures were taken into account. More precisely, the cytoplasm, the nucleus and the nucleolus were modeled as ellipsoidal volumes by considering the various medium compositions, namely, hydrated

DNA for the nucleolus and liquid water with appropriate scale density factor for the two other cellular regions.

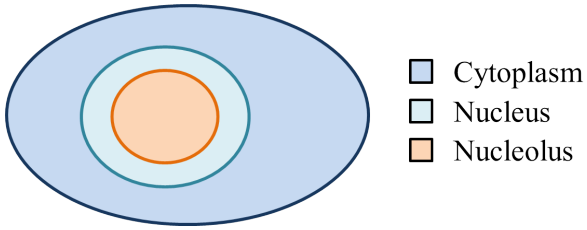

Figure 5. (Color online) Cell geometry model used in *TILDA-V*.

Therefore, when some geometrical objects are implemented into MCTS codes, it is of prime importance to correctly describe the behavior of the particle at the interface for *in fine* being able to mimic the transport of charged particles in any heterogeneous medium. To do that, various approaches were proposed. For more details, we refer the interested reader to the PhD thesis of S. Edel (2006), where the author analyzed several options to treat this problem and pointed out in particular the impact of an atomic description of the DNA macromolecule. Besides, in the major part of the existing Monte Carlo codes, the strategy commonly in use consists in stopping the particle at the interface and then in reconsidering its energy at this point for the following step of tracking (see (Salvat *et al* 2008) for the PENELOPE code). The procedure followed in *TILDA-V* is slightly different.

Let us consider two homogeneous media M_1 and M_2 characterized by their respective density ϱ_1 and ϱ_2 and separated by an interface crossed by a straight-line track of a charged particle moving from the medium M_1 to the medium M_2 (see Figure 6).

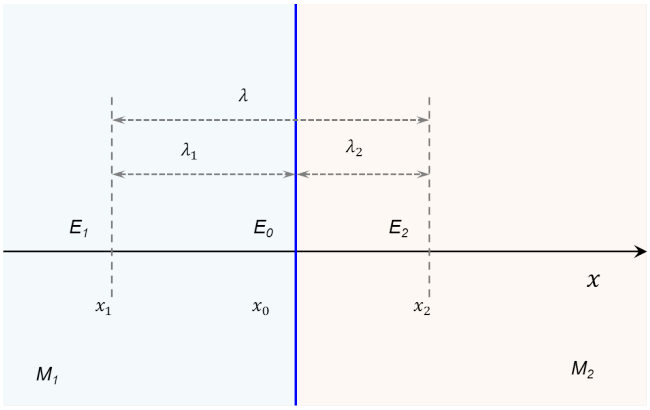

Figure 6. (Color online) Charged particle transport at the interface between two media.

The total mean free path λ is computed as the sum of the mean free paths of the two media (λ_1 and λ_2, respectively). However, the position x_2 does not represent the "right" post-*event* position of the particle due to the difference of densities between the two media. Under these conditions, we applied a rescaling procedure, which consists in using the density ratio $\frac{\rho_1}{\rho_2}$ as a multiplicative factor

$$\lambda_1 = \|x_0 - x_1\| \text{ and } \lambda_2 = \|x_2 - x_0\| \frac{\rho_1}{\rho_2}. \quad (5)$$

Once both distances have been determined, we compute the energy lost by the particle on both sides of the interface by means of the relations

$$E_0 = E_1 - \left(\frac{\Delta E}{\Delta x}\right)_{M_1}(E_1)\cdot\lambda_1$$
$$E_2 = E_0 - \left(\frac{\Delta E}{\Delta x}\right)_{M_2}(E_0)\cdot\lambda_2 \quad (6)$$

where E_0 and E_2 denote the particle energy at the positions x_0 and x_2 and $\left(\frac{\Delta E}{\Delta x}\right)_{M_i}$ refers to the electronic stopping power of the charged particle of interest (proton, hydrogen atom or electron) in the medium M_i (i = 1,2), the latter being interpolated from *pre-calculated* tables for each medium and for a pre-defined list of incident energies (see the section Results and discussion).

TILDA-V is then able to provide the coordinates of all the interactions as well as the type of collision together with the energy transfer (the deposited energy as well as the kinetic energy of the resultant particles), allowing then an accurate dosimetry of proton-beam irradiations in any homogeneous or heterogeneous "realistic" biological entities.

2. Theoretical description of the collisional processes

TILDA-V aims at describing the full proton track structure in water and DNA within the energy range 10 keV-100 MeV including the complete slowing-down of the secondary electrons down to an energy cut-off fixed at 7.4 eV. The current version includes a variety of theoretical models independently developed within the quantum mechanical framework for describing the multiple differential and total cross sections of almost all the electron- and proton/hydrogen-induced interactions in water and DNA components including the nucleobases and the sugar-phosphate backbone (see Table 3). Additionally, *TILDA-V* also includes a selection of semi-empirical models currently in use by some of the existing MTSC (see Table 3) in order to point out the reliability of our quantum mechanical approach. Besides, due to the lack of theoretical support in its present form, *TILDA-V* also includes some semi-empirical models in particular for describing the excitation process in water and DNA for proton, hydrogen and electron impact. Table 3 summarizes all the models actually included in the *TILDA-V* code.

Location of Table 3

Table 3. List of the physical models available in *TILDA-V*.

In the following, we give a brief overview of the theoretical models implemented into *TILDA-V* for describing the main collisional processes induced by proton/hydrogen atom and electron impact in water vapor and DNA. A selection of theory/experiment comparisons is also reported in order to highlight the consistency of the theoretical models as well as their limitations. For more details we refer the interested reader to the related works reported as references (Table 3).

2.1. Proton-induced interactions

2.1.1. Ionization

The ionization process is here described within the independent active electron approximation that consists in considering the passive target electrons (those non-ionized) as frozen in their initial orbitals during the collision process; this is generally assumed to overcome the difficulty of taking into account the dynamical correlation between active and passive electrons, in particular for large molecules like those here investigated. Nevertheless, let us add that for more information about the influence of electron correlation on ionization of atomic targets, we refer the reader to the detailed analysis recently given by Monti *et al* (2009).

Within this approximation, the interaction between the projectile and the passive electrons only affects the trajectory of the incident particle. Consequently, its contribution to the ionization reaction itself is neglected; this is independent of the quantum approximation used for describing the ion-induced ionization process of atoms and molecules, especially since we only consider here calculations of cross sections integrated over the projectile scattering angle. Then, we focus in the following on the theoretical description of the dynamics of the active (ejected) electron.

In the CDW-EIS model, the initial and final distorted wave functions are chosen as

$$\chi_\alpha^+ = \frac{\exp(i\mathbf{K}_\alpha.\mathbf{R})}{(2\pi)^{3/2}}\varphi_\alpha(\mathbf{x})\exp\left[-i\frac{Z_P}{v}\ln(vs+\mathbf{v}.\mathbf{s})\right] \tag{7}$$

and

$$\chi_\beta^- = \frac{\exp(i\boldsymbol{K}_\beta.\boldsymbol{R})}{(2\pi)^{3/2}}\varphi_\beta(\boldsymbol{x})N^*(Z_T^*/k)\,{}_1F_1(-iZ_T^*/k;1;-ikx-i\boldsymbol{k}.\boldsymbol{x})\,N^*(Z_P/p)\,{}_1F_1(-iZ_P/p;1;-ipx-i\boldsymbol{p}.\boldsymbol{x}) \tag{8}$$

where the vectors $\boldsymbol{x}$ and $\boldsymbol{s}$ give the positions of the active electron with respect to the centre of mass of the residual target and to the projectile, respectively, whereas $\boldsymbol{R}$ denotes the position of the projectile with respect to the centre of mass of the target. Furthermore, ε_α denotes the active electron orbital energy, $\boldsymbol{v}$ the collision velocity, $\boldsymbol{k}$ the momentum of the ejected electron seen from the target, $\mathbf{p} = \mathbf{k} - \mathbf{v}$ the momentum of this electron with respect to the projectile, and $\boldsymbol{K}_\alpha$ and $\boldsymbol{K}_\beta$ the momenta of the reduced particle of the complete system in the entry and exit channels, respectively, Z_P being the projectile charge and Z_T^* an effective target charge. In Eq.(2), $N(a) = \exp(\pi a/2)\Gamma(1-ia)$ and $N^*(a)$ indicates the conjugate of $N(a)$.

The function $\varphi_\alpha(\mathbf{x})$ describes the bound electron wave function and the multiplicative projectile eikonal phase in Eq.(7) (depending on the electronic coordinate **s** of the active electron) indicates that the active electron moves simultaneously in a bound state of the target and implicitly in a projectile eikonal continuum one. The eikonal form of the projectile-active electron continuum is chosen to preserve the normalization of the initial distorted wave function. In the exit channel, $\varphi_\beta(\boldsymbol{x})$ is a plane wave that multiplied by the effective Coulomb continuum factor (see Eq.(8)) gives the continuum of the ionized electron in the field of the residual target, while the inclusion of a multiplicative projectile continuum factor indicates that the electron is moving in a continuum state of the residual target and projectile combined fields, both considered on equal footing. Thus, initial and final distorted wave functions in CDW-EIS are

chosen as two-centre ones in the sense that the active electron is considered to feel the simultaneous presence of the projectile and residual target potentials in the entry and exit channels at all distances between aggregates. It avoids the presence of disconnected diagrams associated with the separated consideration of these potentials, which could induce to the presence of divergences in the corresponding Lippmann-Schwinger development. Moreover, CDW-EIS includes in the initial and final distorted wave functions, the long-range Coulomb character of the interaction of the active electron with the projectile in the entry channel and also with the residual target in the exit one, so that they satisfy correct asymptotic conditions in both channels. This property is crucial to avoid the presence of the divergent contribution of the intermediate elastic channel in the ionization reaction. For more details on the distorted initial and final wave functions and the corresponding perturbation potentials, the reader is referred to Stolterfoht *et al* (1997).

In the CB1 model, the initial and final wave functions are chosen as

$$\varphi_\alpha^+ = \frac{\exp(i\boldsymbol{K_\alpha}.\boldsymbol{R})}{(2\pi)^{3/2}}\phi_\alpha(\boldsymbol{x})\exp\left[-i\frac{Z_P}{v}\ln(vR-\boldsymbol{v}.\boldsymbol{R})\right] \tag{9}$$

and

$$\varphi_\beta^- = \frac{\exp(i\boldsymbol{K_\beta}.\boldsymbol{R})}{(2\pi)^{3/2}}\phi_\beta(\boldsymbol{x})N^*(Z_T^*/k)_1F_1(-iZ_T^*/k;1;-ikx-i\boldsymbol{k}.\boldsymbol{x})\exp\left[+i\frac{Z_P}{v}\ln(vR+\boldsymbol{v}.\boldsymbol{R})\right] \tag{10}$$

Let us note that the main difference between the initial wave function described by Eq.(9) and that given in the CDW-EIS approach resides in an eikonal phase depending on $\boldsymbol{R}$ instead of $\boldsymbol{s}$, so that the asymptotic boundary conditions associated with the projectile-active electron interaction are now preserved but φ_α^+ presents a one-target centre character. In the exit channel (see Eq.(10)), an asymptotic version of this interaction is also considered (depending again on $\boldsymbol{R}$), which will be valid under the dynamic condition $k << v\ (x << R)$. So, in the CB1 approximation for ionization, correct boundary conditions are only satisfied in this restricted coordinate space region. Thus, φ_β^- presents also a one-target centre character. It must be also mentioned that the application of the active electron Schrödinger equation on the wave function given in Eq.(9) results in

$$(H_\alpha - E_\alpha)\phi_\alpha^+ = V_\alpha\phi_\alpha^+ \tag{11}$$

with the perturbative potential given by

$$V_\alpha = -\frac{Z_P}{s} + \frac{Z_P}{R} \tag{12}$$

In this expression the second addend term results from the inclusion, in the initial wave function, of the projectile-active electron interaction at large asymptotic separation between both particles. Thus, only the short range part of this interaction contributes to the perturbative potential. It is easy to show that the corresponding eikonal phases appearing in the initial and final wave functions and depending on $\boldsymbol{R}$ in CB1 may be neglected when cross sections integrated over the projectile scattering angle are considered (Champion *et al* 2013).

Additionally, *TILDA-V* gives the opportunity of using semi-empirical models for predicting the ionization process for the biomolecules under investigation. Among them, let us cite the HKS model (Hansen and Kocbach 1989) where doubly and singly differential cross sections are provided within the impact parameter 1st Born approximation by describing the initial and the final electron states by means of a hydrogenic function and a plane wave, respectively. Total cross sections are then obtained by numerical integration. In this model, as well as in the simple Rutherford expression of total ionization cross section (Stolterfoht *et al* 1997), which is also considered in *TILDA-V*, the binding energy of the different subshells of the molecular target under interest represent the only input data needed for the calculations. The latter are obviously taken from the molecular description related in §1.2. On the contrary, the Rudd's model (Rudd 1989), which provides an analytic equation for the secondary electron energy distributions, uses a large set of fitting parameters deduced from experimental data. Some results have already been reported in the literature for water [see for example (Bernal and Liendo 2006)]. Recently, we adapted these three models for DNA ionization and reported a full documented intra-comparison in terms of multiple differential and total cross sections (Champion *et al* 2014).

Figures 7 and 8 depict the total ionization cross sections for water and DNA nucleobases and sugar-phosphate backbone obtained with the various models available in *TILDA-V*. From a general point of view, and as demonstrated in our previous works (Champion *et al* 2010, 2013 and 2014), the present quantum mechanical predictions are in good agreement with the experiment over the entire energy range covered by the simulation, even considering the well-known underestimation of the CDW-EIS model below 50 keV incident as well as the overestimation of the CB1 approach at very low energy (E_{inc} < 20 keV). Besides, let us note that among the semi-empirical approaches currently in use in the existing MCTS codes, the Rudd model appears as the most reproductive one, the HKS formalism exhibiting evident divergences with experiment in particular in the low-energy regime, whereas the Rutherford predictions tend to overestimate the data for 20 keV < E_{inc} < 200 keV (see Figure 7).

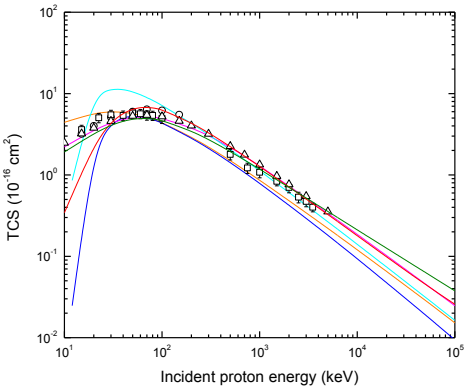

Figure 7. (Color online) Total cross sections for proton-induced ionization in water vapor. Current theoretical predictions (lines): CB1 (orange) and *prior* CDW-EIS (red); semi-empirical predictions (lines): Rutherford (cyan), Green and McNeal (green), HKS (blue) and Rudd (magenta). The experimental data are taken from various sources: Rudd *et al* (1985) (circles), Bolorizadeh and Rudd (1986a) (up-triangles) and Luna *et al* (2007) (squares).

Regarding the DNA nucleobases and the SP backbone ionization cross sections (see Figure 8), a large similarity is observed among all the components considered. Besides, we note that the present theoretical predictions - and more particularly those provided by the *prior* CDW-EIS model - show very good agreement with the experimental data recently reported by Iriki *et al* (2011a, 2011b) for 0.5-, 1- and 2-MeV protons impacting on adenine targets. On the other hand, the data reported by Tabet *et al* (2010) at 80 keV exhibit large discrepancies with our results by a factor of ~2-5.

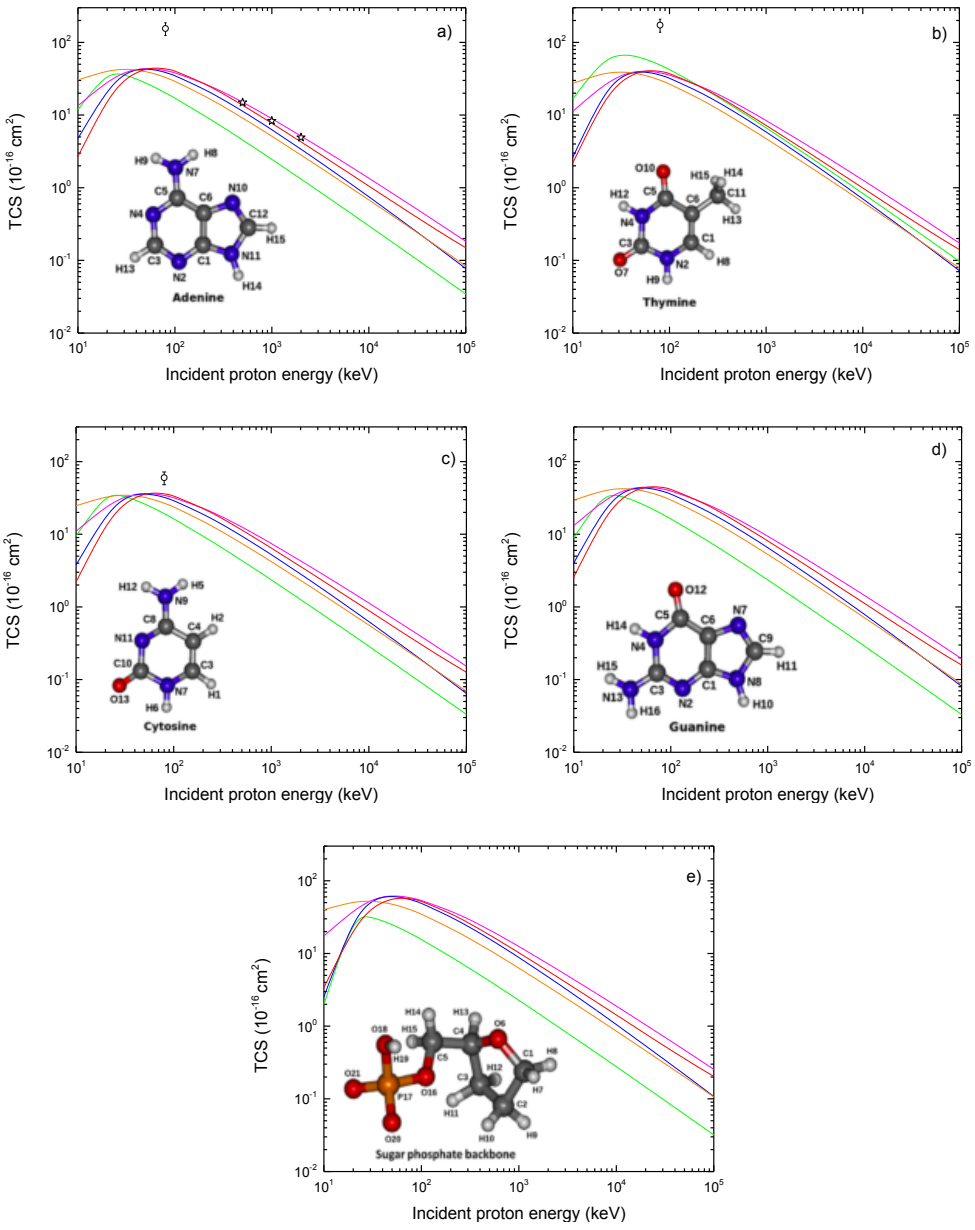

Figure 8. (Color online) Total ionization cross sections for the main DNA components impacted by protons: a) adenine, b) thymine, c) cytosine, d) guanine and e) sugar-phosphate backbone. Theoretical predictions (lines): CB1 (orange) and *prior* CDW-EIS (red); semi-empirical predictions (lines): Rutherford (green), HKS (blue) and Rudd (magenta). The experimental data are taken from Tabet *et al* (2010) (circles) and Iriki *et al* (2011a and 2011b) (stars).

Figures 9 and 10 illustrate the reliability of the two quantum mechanical models implemented into *TILDA-V* for describing the ionization process at the most differential scale. Thus, whether it is in terms of energy transfers (singly differential cross sections, SDCS) or in terms of angular distributions (doubly differential cross sections, DDCS), the current theoretical supports exhibit a very good agreement with the

existing measurements. More precisely, the experimental SDCS reported in Figs. 9a and 10a are very well reproduced provided that the ejected electron remains lower than about 10 eV, which roughly corresponds to the energy cut-off for the following-up of the secondary electrons. In this context, the CB1 model exhibits the best agreement, the CDW-EIS as well as the two semi-empirical models showing a larger overestimation in the low-energy regime. Regarding the angular distributions reported in Figs.9b and 10b, we note that the CB1 and the CDW-EIS both reproduce very well the existing data except in the forward and the backward directions ($\theta_e < 20°$ and $\theta_e > 120°$, respectively) where the measurements are systematically underestimated by all the theories as well by the semi-empirical HKS model. Fortunately, this shortcoming has limited impact on the proton tracking since corresponding to cases of relatively low probability of occurrence.

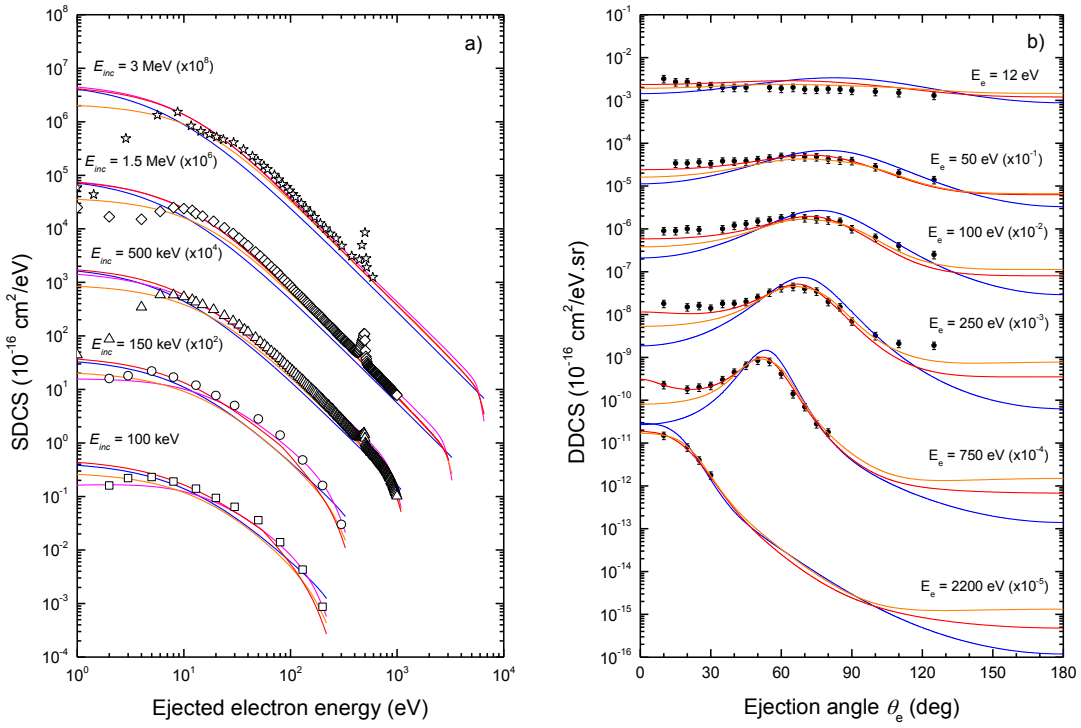

Figure 9. (Color online) a) Singly differential cross sections for proton-induced ionization in water vapor. Theoretical predictions (lines): CB1 (orange) and *prior* CDW-EIS (red); semi-empirical predictions (lines): HKS (blue) and Rudd (magenta). The experimental data are taken from Toburen and Wilson (1977) (up-triangles (E_{inc} = 0.5 MeV), stars (E_{inc} = 3 MeV) and diamonds (E_{inc} = 1.5 MeV)) and from Bolorizadeh and Rudd (1986a) (squares (E_{inc} = 100 keV) and circles (E_{inc} = 150 keV)). b) Doubly differential cross sections for 1 MeV proton in water and for different ejection energies E_e. Theoretical predictions (lines): CB1 (orange) and *prior* CDW-EIS (red), HKS (blue). The experimental data (circles) are taken from Toburen and Wilson (1977). Scaling factors are used for clarity reasons.

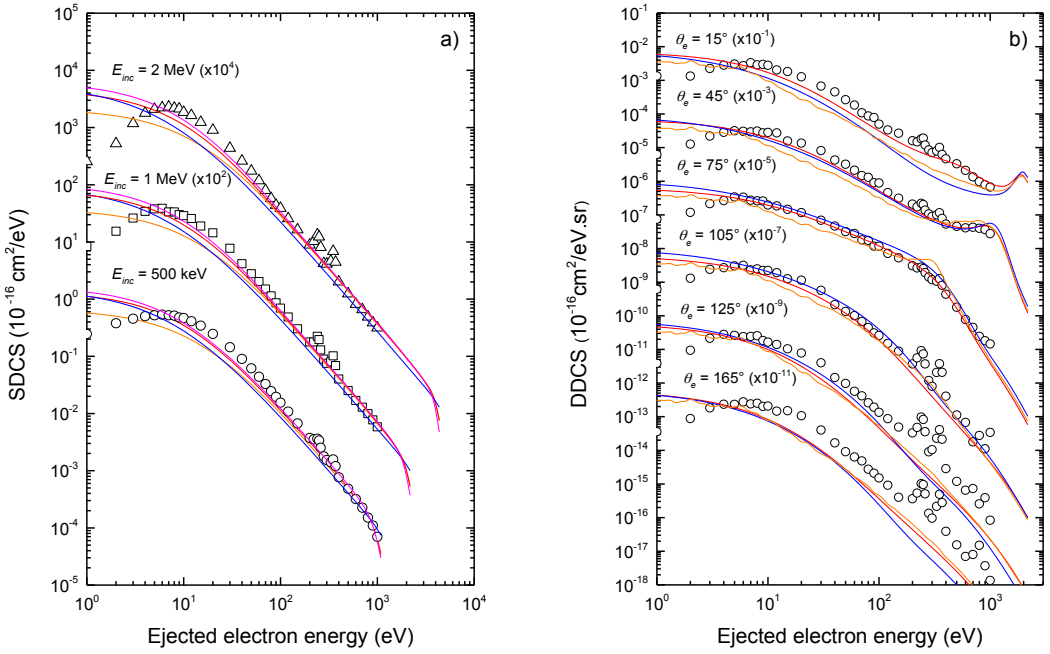

Figure 10. (Color online) a) Singly differential cross sections for proton-induced ionization of adenine. Theoretical predictions (lines): CB1 (orange) and *prior* CDW-EIS (red); semi-empirical predictions (lines): HKS (blue) and Rudd (magenta). The experimental data are taken from Iriki *et al* (2011a, 2011b): circles (E_{inc} = 500 keV), squares (E_{inc} = 1 MeV) and up-triangles (E_{inc} = 2 MeV). Scaling factors are used for clarity reasons. b) Doubly differential cross sections for 1 MeV proton in adenine and for different ejection energies. Theoretical predictions (lines): CB1 (orange) and *prior* CDW-EIS (red); semi-empirical predictions (lines): HKS (blue). Experimental data (circles) are taken from Iriki *et al* (2011a). Scaling factors are used for clarity reasons.

2.1.2. Electron capture

Similarly to the ionization process, the single electron reaction is described in *TILDA-V* within the framework of the independent electron model approach, which considers the passive electrons (the target electrons not captured during the reaction) to remain frozen in their initial molecular orbital. The multi-electronic problem is then reduced to a mono-electronic one involving three effective bodies, namely the projectile, the active electron and the residual target. Under these conditions, only the active electron that is captured during the process of interest is considered.

In *TILDA-V*, the electron capture total cross sections are computed within the distorted wave model by two different approaches, namely, the continuum distorted wave (CDW) (Cheshire 1964, Belkić *et al* 1979) and the continuum distorted wave-eikonal initial state (*post* CDW-EIS) models (Martínez *et al* 1989, Abufager *et al* 2004). Let us note that these two-centre models both satisfy the correct asymptotic boundary conditions describing the active electron in the simultaneous presence of both the projectile and residual target fields acting as two effective Coulomb centers in both the initial and final channels of the reaction. Moreover, it is well known that a proper description of electron capture requires the inclusion of Born terms higher than the second one (Miraglia *et al* 1981). This requisite is verified by the CDW and CDW-EIS

models since the distorted wave method contains high-order Born effects through the implicit inclusion of continuum intermediate states. In fact, the difference between the CDW-EIS and CDW models essentially lies in the description of the initial channel. Indeed, in the CDW model the active electron is described as bound to the target but simultaneously in a continuum state of the projectile field while in the CDW-EIS approximation this Coulomb function is replaced by its asymptotic limit, namely the eikonal phase. This last choice allows the use of normalized initial distorted wave functions which avoids the typical overestimations of the total cross sections provided by the CDW model at intermediate and low impact energies.

Besides, similarly to the ionization case, semi-empirical models were also implemented into *TILDA-V*, essentially for water since to the best of our knowledge the only theoretical support of the electron capture on DNA was given in our recent work (Champion *et al* 2012b). Among the semi-empirical approaches available in the literature, we first considered the approach proposed by Rudd *et al* (1985), which consists in expressing the charge transfer cross section σ as $\sigma = \sigma_+ - \sigma_-$ by means of adjustable parameters deduced by fitting measured cross sections of positive (ion) and negative (electron) charge production (σ_+ and σ_-, respectively). Additionally, we also considered the model suggested by Dingfelder *et al* (2000), where the charge transfer cross sections are expressed by analytical formula by means of fitting parameters deduced from various sources of experiments (Toburen *et al* (1968) and Dagnac *et al* (1970)). Finally, we also implemented a third model based on the analytical functions developed by Green and McNeal (1971), who fitted the experimental data of Toburen *et al* (1968).

Figure 11 reports a comparison between the predictions provided by the different models in terms of total cross sections for both water and DNA components. For water (see Fig.11a) we observe that among the two current distorted wave models developed here, the best agreement is observed with the CDW-EIS approach, the CDW model exhibiting a large overestimation of the experimental total cross sections for proton energies lower than about 100 keV. Besides, the predictions provided by the Green and McNeal model as well as those given by the Dingfelder model show a very good agreement with the data, contrary to the Rudd's approach, which largely overestimates the experiment in the energy range of interest, namely, for $E_{inc} > 100$ keV. Considering now the DNA case, Fig.11b shows a comparison between the CDW and CDW-EIS results and the rare existing measurements. Similarly to the ionization case above, we observe that the data reported by Tabet *et al* (2010) at 80 keV exhibit a large discrepancy with our results of about one order of magnitude, a tendency that has been recently confirmed by the calculations performed by Privett and Morales within the electron nuclear dynamics (END) framework (Privett and Morales 2014). In their work, the authors developed two independent END models coupled with various types of basis sets for describing the biomolecular targets and demonstrated the ability of their theories to accurately describe the one-electron transfer process for proton-induced collisions on A, C, T and U nucleobases.

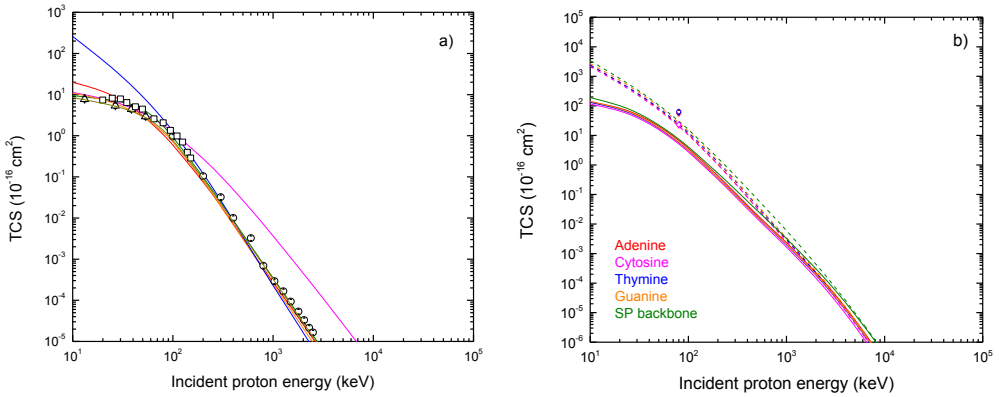

Figure 11. (Color online) a) Total cross sections for proton-induced capture in water vapor. Theoretical predictions (lines): *prior* CDW-EIS (red) and CDW (blue); semi-empirical predictions (lines): Rudd (magenta), Green and McNeal (1971) (green), Miller and Green (1973) (dark yellow) and Dingfelder *et al* (2000) (orange). The experimental data are taken from various sources: Dagnac *et al* (1970) (up-triangles), Gobet *et al* (2001) (squares) and Toburen *et al* (1968) (circles). b) Total cross sections for proton-induced capture on the main DNA components. Theoretical predictions: *post* CDW-EIS (solid lines) and CDW (dashed lines). The experimental data are taken from Tabet *et al* (2010).

2.1.3. Excitation induced by proton

Due to the scarcity of experimental checkpoints for modeling the excitation process, the existing MCTS codes developed in the last decades are mainly based on the semi-empirical approach proposed by Miller and Green (1973), which consists in a velocity scaling of the electron-induced excitation cross sections together with extensions towards lower proton energies (see for example Uehara *et al* (2000)). In their model, the authors reported a large set of fitting parameters for simulating the proton-induced excitation cross sections for 28 excited states of the water molecule. In *TILDA-V*, we have adopted an extension of this model described by Dingfelder *et al* (2000), who suggested a slightly modified set of parameters so that the semi-empirical approach agrees in the high-energy limit with the 1st Born approximation predictions. Figure 12 displays the total excitation cross section (red line) together with the contribution of the five excited states included in the semi-empirical approach of Dingfelder *et al*, namely, the $\tilde{A}^1B_1$, the $\tilde{B}^1A_1$, the Rydberg A+B, the Rydberg C+D and the diffuse bands.

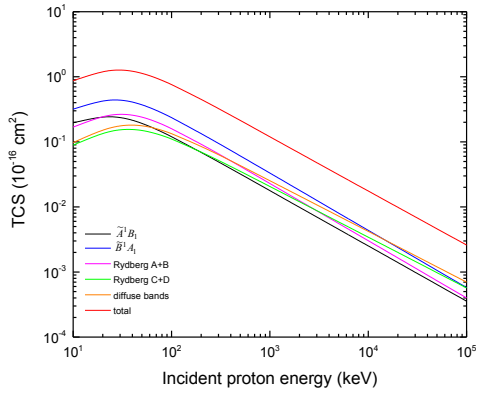

Figure 12. (Color online) Total excitation cross sections for proton in water.

For DNA components, a similar procedure of velocity scaling of electron-induced excitation cross sections was followed. To do that, we used experimental total cross sections of electron-induced excitation of DNA components (essentially on thymine, see hereafter the section dedicated to electron-induced excitation cross sections) to extrapolate the fitting parameters (α, β, Ω and K) needed in the semi-empirical formula suggested by Miller and Green (1973) for modeling the proton-induced excitation

$$\sigma_{exc}(E) = \frac{(Za)^{\Omega}\,(E-W)^{\upsilon}}{J^{\Omega+\upsilon} + E^{\Omega+\upsilon}} \tag{13}$$

where

$$J = C_2\,\frac{M_p}{m_e}\,W\left(\frac{a\beta+\Omega}{\Omega}\right)^{1/\beta}\left(\frac{\Omega}{\upsilon}\right)^{1/(\Omega+\upsilon)} \tag{14}$$

and

$$a = C_2\,\frac{M_p}{m_e}\,\frac{W}{Z}\left[\frac{C_1\widetilde{K}}{W^2}\left(\frac{\upsilon+\Omega}{\upsilon}\right)\left(\frac{\alpha\beta}{\alpha\beta+\Omega}\right)^{\alpha}\right]^{1/\Omega} \tag{15}$$

with $C_1 = 4$, $C_2 = 0.25$, $\upsilon = 1$ and $\Omega \approx 1$ as suggested by Miller and Green (1973). The coefficient $\widetilde{K}$ was computed from the parameter K as $\widetilde{K} = Kq_0$.

Let us add that in Eq.(13) Z designates the number of target electrons while W is an adjustable value of the excitation threshold. Here, we used $W = 4$ eV. Finally, in Eqs.(14-15) M_p and m_e refer to the proton and the electron mass, respectively.

Location of Table 4

Table 4. Fitting parameters for the total cross sections of proton-induced excitation of DNA.

Figure 13 reports the total cross sections obtained for the various DNA components investigated here.

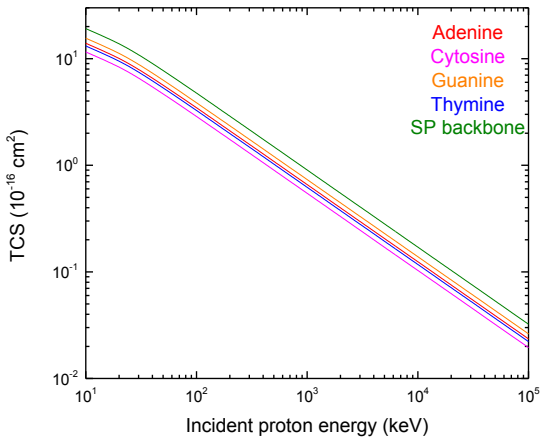

Figure 13. (Color online) Total excitation cross sections for proton in DNA.

2.1.4. Elastic scattering

The proton-induced elastic scattering process is here treated within the classical mechanical framework where the DDCS are given by the well-known relation

$$\frac{d\sigma}{d\Omega} = -\frac{p}{\sin\theta}.\frac{dp}{d\theta}, \tag{16}$$

where p refers to the impact parameter whereas θ denotes the scattering angle in the centre-of-mass system, the latter being defined by

$$\theta = \pi - 2\int_{r_{\min}}^{\infty} \frac{p}{r^2\sqrt{1-V(r)/E_{inc}^{CM} - p^2/r^2}}dr, \tag{17}$$

where r_{min} is the distance of closest approach and E_{inc}^{CM} the incident particle energy in the centre-of-mass system.

Let us add that the interaction potential $V(r)$ has been numerically calculated from the respective target wave function for both water and DNA (see Fig.14 a). Total cross sections are then obtained by numerical integrations of the DDCS over the scattering solid angle $d\Omega = 2\pi\sin\theta.d\theta$. Let us mention that the numerical integration of Eq.(17) has to be carefully performed by using a fine logarithmic radial grid in order to avoid any overestimation of the obtained scattering angle. In the same way, the numerical integrations over the scattering solid angle were performed by using a cut-off angle θ_{cut} in order to reduce the divergence due to the high DDCS at low scattering angles (see Uehara *et al* 2001). We hereafter report some preliminary results in terms of doubly differential cross sections (see Fig.14 b) and for more details we refer the reader to our forthcoming work where a detailed analysis of the scattering process will be given for proton in both water and DNA (Champion and Quinto, 2016).

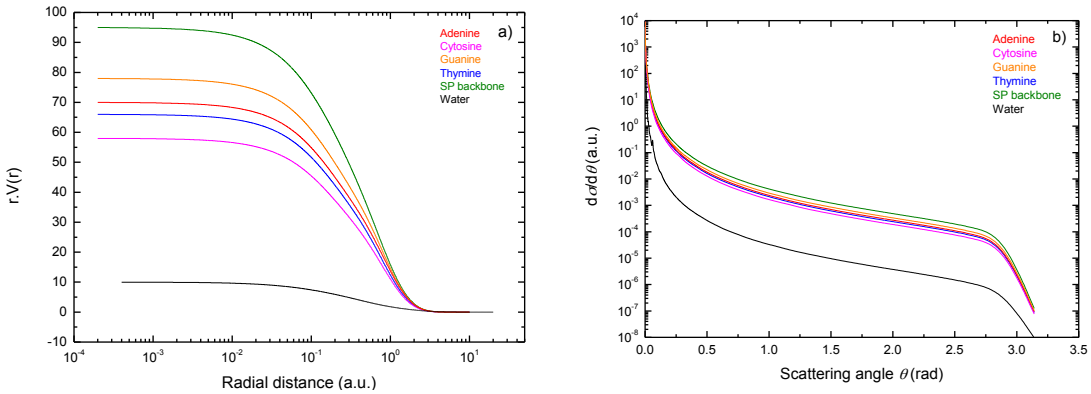

Figure 14. (Color online) Elastic scattering of proton in water and DNA. a) Interaction potential between an incident proton and the biological target of interest; b) Singly differential cross sections for 100 keV protons in water and DNA.

3.2. Neutral-hydrogen-induced interactions

An accurate knowledge of the neutral-hydrogen-induced interactions is all the more important that in the close vicinity of the Bragg peak (BP), namely, for proton energies around and below 100 keV, the electron capture becomes of the same order of magnitude, or even more important, than the ionization leading then to a substantial amount of atomic hydrogen in the projectile beam. Below 30 keV, the BP is even dominated

almost entirely by the electron capture process. Consequently, it is of prime importance to access to a fine description of the various interactions induced by neutral-hydrogen atoms in the biological matter.

3.2.1. Ionization

Despite their importance, the cross section measurements for water ionization by neutral-hydrogen impact remain to the best of our knowledge extremely rare. In this context, let us cite the first total electron loss cross sections for 100-2500 keV hydrogen atoms in water reported by Toburen *et al* (1968). Later on, Bolorizadeh and Rudd (1986b) measured doubly differential cross sections for electron production in collisions between neutral hydrogen and water molecules at 20-150 keV from which they deduced total *electron production* cross sections. However, without detecting the charge state of the impacted target, the authors were unable to discriminate between the pure target ionization by hydrogen atoms and the stripping process. More recently, Gobet *et al* (2006) and then Luna *et al* (2007) carried out cross section measurements for the ionization of water molecules by 20-150 keV and 8-100 keV neutral hydrogen impact, respectively.

Thus, in the absence of experimental data available for comparison, many semi-empirical models were proposed among which we distinguish the approach suggested by Dingfelder *et al* (2000) who used the same secondary-electron spectrum for proton and neutral-hydrogen impact as a starting point but slightly modified by a scaling function that depends only on the incident particle energy and not on the energy transfer. Based on the data of Bolorizadeh and Rudd (1986b) and of Toburen and co-workers (1968), this scaling function was assumed to be higher than unity at low incident energies and lower than unity for higher energies, in view of the screening of the nuclear charge by the bound electron in hydrogen. Similarly, Uehara *et al* (2000) parameterized the neutral-hydrogen ionization of water molecules by integrating twice the DDCS provided by Bolorizadeh and Rudd (1986b). However, the total cross section also obtained including the contributions of electrons ejected from both the target and the projectile, the authors suggested to subtract the electron loss contribution and reported an analytical expression for the total cross section of the hydrogen-induced ionization within the 20-150 keV energy range. Beyond this range, the hydrogen cross sections are simply scaled from the proton ones by a factor close to unity. Finally, let us cite the model developed by Green and McNeal (1971) that uses an analytical expression similar to that proposed for the proton-induced ionization with fitting parameters deduced from hydrogen experiment in H_2 and O_2.

In *TILDA-V* we aimed at going beyond this empirical approach by using the 1st quantum mechanical model of the neutral-hydrogen-induced ionization we recently reported for both water and DNA. The CB1 and prior CDW-EIS approximations are then used as theoretical support allowing a fine description of the ionization process in terms of differential and total cross sections. Let us point out that the current approach clearly differs from the *above-cited* semi-empirical approaches, which all assumed that the angular and the energetic spectra were similar for both protons and hydrogen atoms. An illustration of the preliminary theoretical predictions in terms of total cross sections is reported for water and DNA in Figure 15. For more details we refer the reader to our forthcoming work (Champion *et al* 2016).

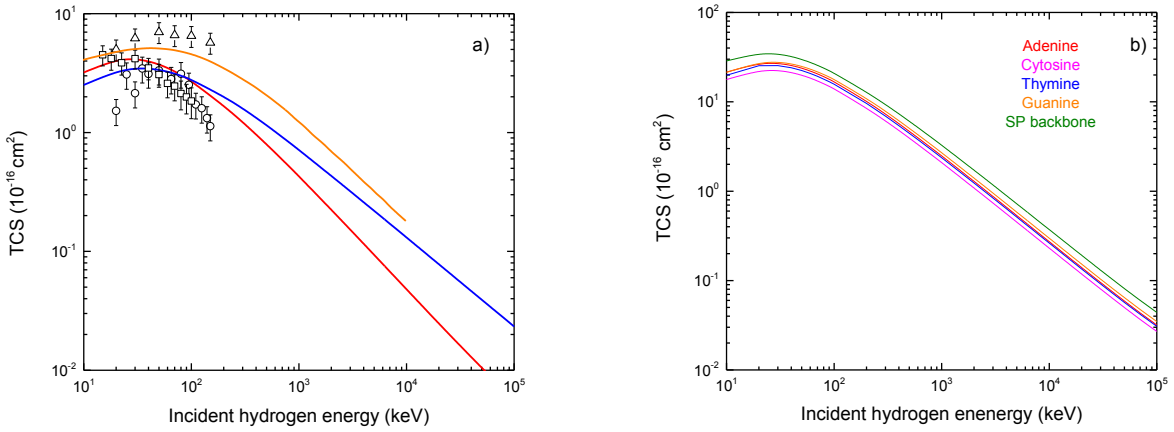

Figure 15: (Color online) a) Total ionization cross sections for hydrogen atom in water vapor. *Prior* CDW-EIS predictions (red) compared with semi-empirical approaches from Green and McNeal (1971) (orange) and Dingfelder *et al* (2000) (blue). The experimental data are taken from: Gobet *et al* (2006) (circles), Luna *et al* (2007) (squares) and Bolorizadeh and Rudd (1986b) (triangles). b) Total ionization cross sections for hydrogen atom in DNA calculated within the *prior* CDW-EIS framework.

3.2.2. Electron capture

As mentioned above, the current version of *TILDA-V* neglects the hydrogen-induced electron capture process (which leads to a negative H^- ion formation), owing to its very low probability of occurrence. Indeed, in their recent work Abicht *et al* (2013) reported experimental and calculated cross sections for various projectile charge transfer processes in water vapor and clearly showed that the cross section of the negative ion H^- production was at least one order of magnitude lower than the hydrogen-induced electron loss process. Under these conditions, we neglected this process and never considered any negative ions in our simulations.

3.2.3. Excitation induced by neutral-hydrogen

Contrary to Dingfelder *et al* (2000) who neglected the neutral-hydrogen-induced excitation process in view of lack of experimental or theoretical support, we followed in *TILDA-V* the approach of Uehara *et al* (2000) who assumed that the neutral-hydrogen cross sections could be expressed by the same analytical expression in which they simply changed one of the fitting parameters, namely, the parameter a equal to $3/4$ of the proton value (Miller and Green 1973). Nevertheless, the authors clearly mentioned that the cross sections also provided should be seen as roughly estimates in particular in absence of experimental or theoretical data.

Similarly, the neutral-hydrogen total excitation cross section on DNA components has been computed by using the proton-induced excitation cross section formula reported in Eq.(13) with the same coefficients listed in Table 4 except the parameter a which has been rescaled by a factor 3/4. The obtained values used are reported hereafter in Table 5.

Location of Table 5

Table 5: Parameters used for the hydrogen-induced excitation in DNA.

3.2.4. Elastic scattering

In the absence of experimental data as well as theoretical support, we have followed the suggestion of Endo *et al* (2002) who analyzed the theoretical calculations reported by Krstic and Schultz (1998) for the $H^0 + H_2$ and the $H^+ + H_2$ systems and then suggested to fit the hydrogen *vs* proton cross section ratio by

$$\frac{\sigma_{H^0}}{\sigma_{H^+}} = 1 + 0.0224\log(E) + 0.01285 * \log(E)^2 \qquad (18)$$

that leads to a ratio close to unity within the incident energy range here considered.

3.3. Secondary electron tracking

3.3.1 Electron-induced interactions in water

All the secondary particles emitted along the various ionizing processes (ionization, electron loss) are followed step by step with a *home-made* Monte Carlo code, called *EPOTRAN* (an acronym for Electron and Positron Transport in liquid and vapor water) (Champion *et al* 2012a), which presents the particularity of being exclusively based on theoretical cross sections calculated within the quantum mechanical framework (Champion 2003). For more information, we refer the interest reader to the references cited along this paragraph and report hereafter a brief overview of the theoretical support of all the electron-induced events.

Regarding the elastic scattering process, the calculations are performed within the partial-wave formalism by means of a parameter-free model potential adding to exchange and correlation–polarization contributions a static potential numerically deduced from the above-cited molecular wave functions provided by Moccia (1964) for the water vapor and from experimental measurements of electron density auto-correlation functions (Neuefeind *et al* 2002) for the liquid water. Doubly differential and total cross sections were then reported in a comparative study between electron and positron in gaseous and liquid water (see Aouchiche *et al* 2008). We report in Figure 16 a brief overview of the fairly good agreement obtained in terms of differential and total cross sections.

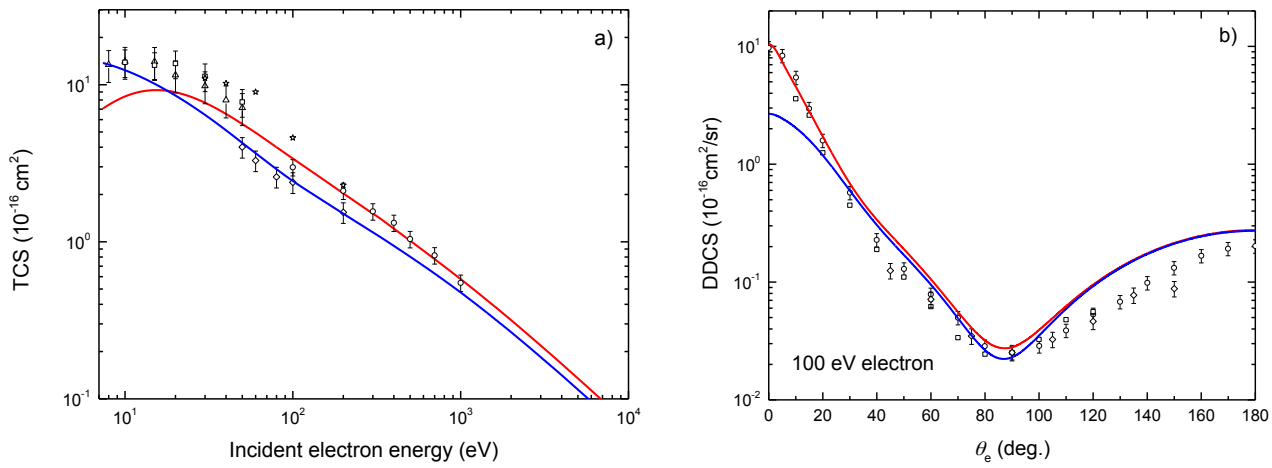

Figure 16. (Color online) Elastic scattering cross sections for electron in water. a) Total cross section for electron scattering in water: the current theoretical predictions for both liquid and gaseous water (blue and red line, respectively) are compared to existing data in water vapor (circles: Katase *et al* 1986, diamonds: Nishimura *et al* 1988, squares: Johnstone *et al* 1991, stars: Shyn and Grafe 1992, triangles: Cho *et al* 2004); b) Doubly differential cross section for 100 eV-electron in water: the current theoretical predictions for both liquid and gaseous water (blue and red line, respectively) are compared to existing data in water vapor (diamonds: Hilgner *et al* 1969, squares: Danjo *et al* 1985, circles: Katase *et al* 1986).

Considering the electron-induced ionization, *EPOTRAN* is based on multiple differential and total ionization cross section calculations performed within the distorted wave Born approximation framework (DWBA), where the incident and scattered (fast) electrons are described by a plane wave function whereas the ejected (slow) electron is described by a distorted wave function. Thus, from five-fold differential cross sections $\frac{d^5\sigma}{d\Omega_s d\Omega_e dE_e}$, namely, differential in the scattering direction, differential in the ejection direction and differential in the ejected energy transfer, the theoretical model also developed is able to provide accurate information in terms of multiple differential and total (integrated) cross sections whose agreement has been checked by many experimental/theoretical confrontations at various scales. An example is reported in Figure 17 and for more details we refer the reader to or previous works (Champion *et al* 2002a, 2002b, 2006, Milne-Brownlie *et al* 2004). Fig.17a shows a comparison between the DWBA predictions in terms of triply differential cross sections with *relative* experimental measurements in the case of 250 eV electron impinging on the $1b_2$ orbital of the water molecule and ejecting an electron of 10 eV. The geometry is here coplanar with a detection (scattering) angle fixed at 45°. Let us remind that in such experiments, the scattered electron is assumed to be the faster one in the *post-collisional* state. In Fig.17b, we have reported a comparison between theory and experiment in terms of doubly differential cross sections (DDCS) for an incident energy E_{inc} = 500 eV while Fig.18c reports on singly differential cross sections (SDCS) for a large panel of incident energies.

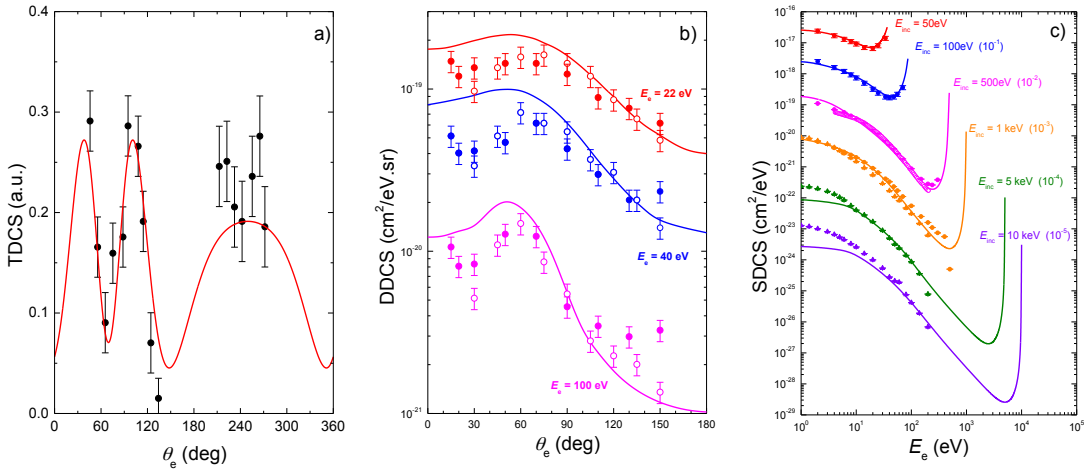

Figure 17. (Color online) Ionization cross sections calculated within the DWBA (solid lines) for electron in water. a) Triply differential cross sections (TDCS expressed in atomic units, a.u.) for the $1b_2$ orbital of the water molecule

impacted by a 250 eV electron with an ejected electron of 10 eV detected in the $\theta_s = 45°$ direction ($\varphi_e = \varphi_s = 0°$) (Champion *et al* 2006); b) Doubly differential cross sections for a water molecule impacted by a 500 eV electron ($\varphi_e = 0°$) (Champion *et al* 2002b); c) Singly differential cross sections of water for various incident energies (Champion *et al* 2012b). Comparison is given with experimental data whose references may be found in our previous works.

At this stage, it is important to underline that the *EPOTRAN* code and then by extension the *TILDA-V* code give access to a *full-differential* modelling of the ionization process contrary to the Monte Carlo codes available in the literature, mostly limited to singly differential and total cross sections. In this case, the angular distributions of the scattered and the ejected electrons are simply deduced from kinematical considerations based on conservation laws, whose main assumption consists in assuming that the secondary electron is ejected in the moment transfer direction. Under these conditions, a *unique* ejection direction θ_e is provided contrary to our case where angular distributions are taken into account. An example is reported in Fig.18, where it clearly appears such an approximation fails to describe the real electron emission.

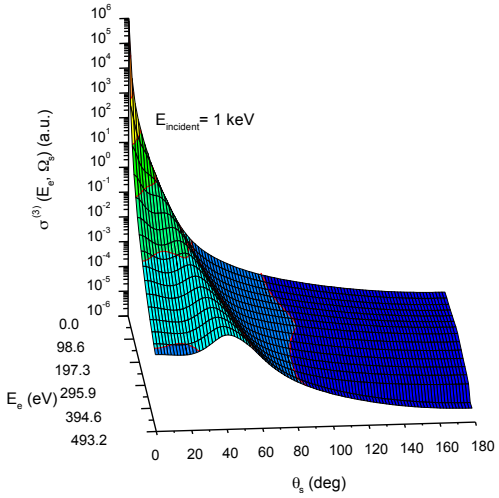

Figure 18. (Color online) Secondary electron angular and energetic distributions for a water molecule impacted by 1 keV electron (Champion *et al* 2002b).

In this context, let us mention the semi-empirical model proposed by Kim and Rudd (1994) - the Binary-Encounter-Bethe (BEB) model with its more recent relativistic extension (Kim *et al* 2000) - which is commonly used for modeling the electron-induced ionization. In this semi-empirical approach, the only needed parameters are the binding energy and the average kinetic orbital energy of all the molecular subshells of the irradiated medium. However, this model remains limited to singly differential and total predictions and then completely neglects the *post-collisional* angular distributions as reported in Figure 18.

Finally, let us add that the original DWBA calculations of electron-induced ionization - initially developed for water vapor - were recently extended for liquid water by means of a unified methodology proposed by Champion (Champion 2010) to express the molecular wave functions of water in both vapor and liquid phases by means of a single centre approach. These latter were then used as input data in the

DWBA treatment reported above and successfully tested for describing the water ionization process in liquid and gaseous water. An example is reported in Figure 19 in terms of total cross section.

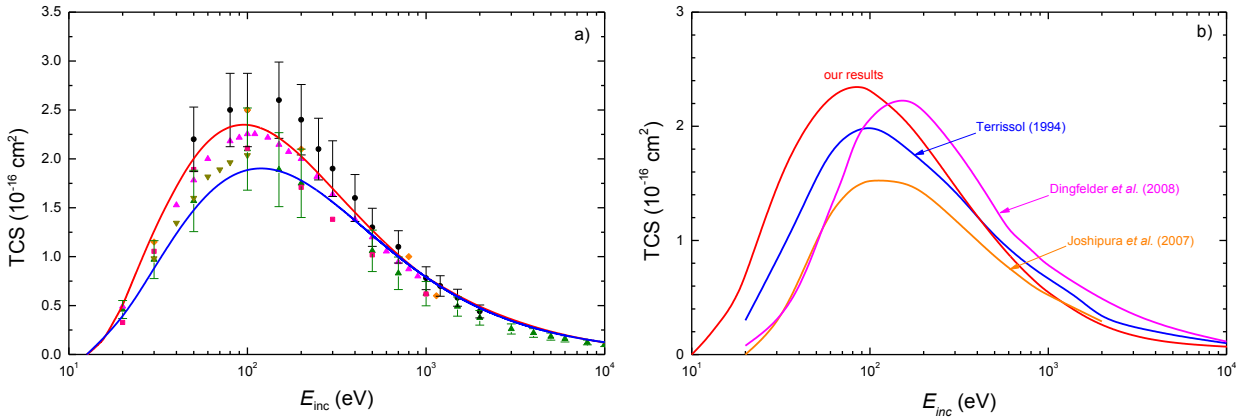

Figure 19. (Color online) Total ionization cross sections for electron in water. a) *Water vapor*: the current DWBA predictions (red line, Champion *et al* 2002a, 2006) are compared with the BEB model results (blue line, Kim and Rudd 1994) as well as existing data; b) *Liquid water*: the current DWBA predictions (red line, Champion 2010) are compared with existing data. Comparison is given with experimental data whose references may be found in our previous works.

Finally, the electron-induced excitation process was taken into account by considering all the *post-collisional* channels that include *i)* the electronic transitions towards Rydberg states or degenerate states ($\tilde{A}_1B_1$, $\tilde{B}_1A_1$, diffuse band), *ii)* the dissociative attachment leading to the formation of negative ions, *iii)* the dissociative excitation leading to excited radicals (H∗, O∗ and OH∗) and in a minor part *iv)* the vibrational and rotational excitation. All these processes give a non-negligible contribution to the energy deposition processes and are then modeled in *EPOTRAN* by the semi-empirical approach of Olivero *et al* (1972) based on experimental data in water vapor and that provides analytic expressions of the total cross sections for all the processes listed in *i)*, *iii)* and *iv)*. Similarly, the expressions reported by Green and Dutta (1967) were used for modeling the dissociative attachment process. All these total cross sections are reported in Figure 20.

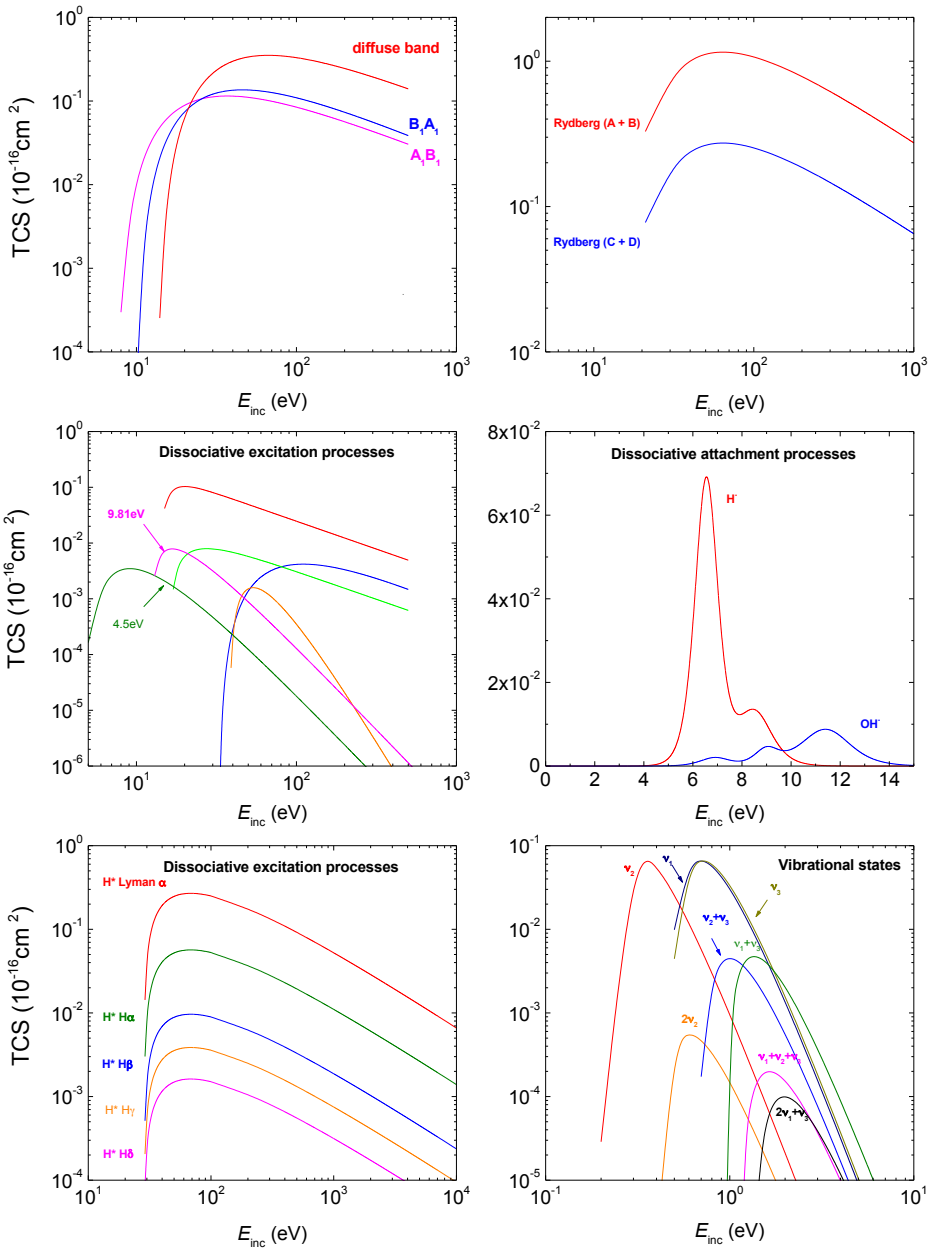

Figure 20. (Color online) Various channels considered in the electron-induced excitation of water vapor.

3.3.2. From water to DNA

a) Ionization

To overcome the usually adopted artifice that consists in using water as a surrogate for biological matter, we recently proposed a quantum mechanical model to describe the electron-induced ionization of DNA components (Champion 2013). In the latter, the ionization process is described within the 1st Born approximation by using a similar partial-wave expansion formalism than that reported above for studying the electron-induced ionization of water. However, contrary to the previous case where the target could be easily described by means of single-centre wave functions (in particular due to the existence of a heavy central atom in the water molecule), the DNA components - being more complex molecules - were treated by means of linear combinations of atomic orbitals. Under these conditions, the multiple differential - and consequently the total (integrated) cross sections - were expressed as linear combinations atomic cross sections corresponding to the various atomic components of the DNA constituents, namely, H_{1s}, C_{1s}, C_{2s},

C_{2p}, N_{1s}, N_{2s}, N_{2p}, O_{1s}, O_{2s}, O_{2p}, P_{1s}, P_{2s}, P_{3s}, P_{2p}, and P_{3p} (see description reported in §1.2 and for more details we refer the reader to (Champion 2013)). In this context, we modified the previously described DWBA model into a CBA (Coulomb Born approximation) model where the ejected electron is modelled by a Coulomb wave function with an effective target charge $Z_T^* = \sqrt{-2n^2\varepsilon}$, where n refers to the principal quantum number of each atomic orbital component used in the molecular target description while the active electron orbital energy ε is related to the ionization energies B of each occupied molecular orbital by $\varepsilon = -B$.

An illustration is reported in Figure 21 for the particular case of the electron-induced ionization of the pyrimidine target, the latter being considered as the precursor of cytosine and thymine and then commonly used as a molecular model to investigate electron-DNA collisions.

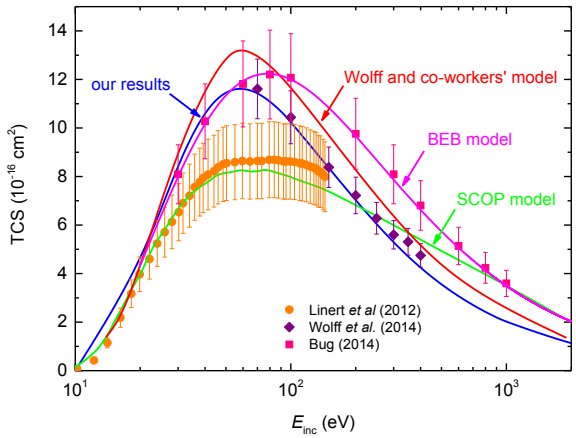

Figure 21. (Color online) Total ionization cross sections for electron in pyrimidine.

b) Excitation

To overcome the scarcity of literature dedicated to electron-induced excitation of DNA components, which is - to the best of our knowledge - limited to the work of Levesque *et al* (2005) on thymine, of Panajotović *et al* (2007) on adenine and of Bazin *et al* (2010) on cytosine, a semi-empirical approach based on an analytical expression of the total excitation cross section was utilized, namely,

$$\sigma_{excit}(E) = q_0 \frac{K}{W^2}\left(\frac{W}{E}\right)^{\Omega}\left[1-\left(\frac{W}{E}\right)^{\beta}\right]^{\alpha} \qquad (17)$$

where E denotes the incident electron energy, W the excitation energy (here seen as an adjustable parameter), q_0 a constant value equal to 651.4 (Olivero *et al* 1972) and α, β, Ω, K fitting parameters.

Thus, by means of least-square fitting of the experimental data of Levesque *et al* (2005), we obtained the values for thymine: $\alpha = 3.8$, $\beta = 2$, $\Omega = 0.7236$, $K = 0.2985$ and $W = 4$ eV. Then, the cross sections for the other DNA components were simply deduced from scaling factor deduced from the respective number of target electrons. The latter was taken into account via the parameter K ($K = 0.3166$, $K = 0.2623$, $K = 0.2528$, and $K = 0.4342$ for adenine, cytosine, guanine and sugar phosphate, respectively). Considering the mean excitation threshold, needed to estimate the energy deposit during the electron-induced excitation, we used either an average energy estimated from the experimental values reported by Michaud *et al* (2012) or a

theoretical value taken from the theoretical work provided by Fleig *et al* (2007) within a quantum-mechanical framework based on coupled cluster methods (see Table 6). Besides, in view of the absence of data for the sugar phosphate group, we used the value of 7.56 eV reported by Bremner *et al* (1991) for the tetrahydrofuran molecule, the latter being commonly used as a simple model of the deoxyribose building block.

Location of Table 6

Table 6. Mean excitation energies (in eV) used in *TILDA-V*.

Figure 22 shows the total excitation cross sections as considered in *TILDA-V* for all the DNA components.

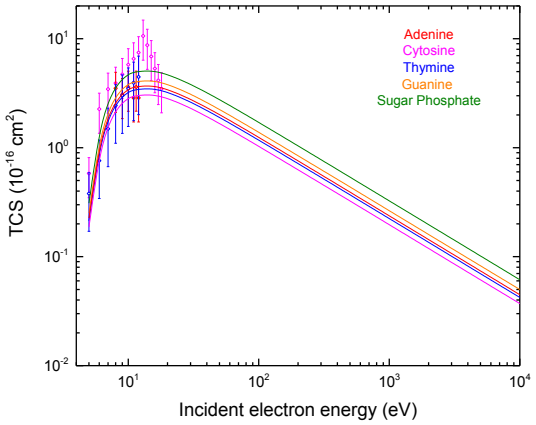

Figure 22. (Color online) Total excitation cross sections for electron in DNA. Experimental data are taken from several sources (thymine: Levesque *et al* 2005, adenine: Panajotović *et al* 2007, cytosine: Bazin *et al* 2010). For a complete review, we refer the reader to the recent work of Michaud *et al* (2012).

4. Results and discussion

In its current form, the *TILDA-V* code comprises a series of theoretical models and, as mentioned above, a selection of semi-empirical approaches essentially used to overcome the lacking of theoretical support for a few processes. Among them, let us first mention the proton-induced electron loss process (usually called stripping) whose relevance may be crucial in the low-energy regime. We are actually working on the extension of our present theoretical models (Born as well as CDW-EIS) to the description of this projectile ionization process but divergences are still observed between the present theoretical predictions and the rare experimental data. More efforts are still needed and we hope to converge rapidly. Similarly, theoretical developments are also in progress for describing the double ionizing processes, namely, the double ionization and the ionization transfer (ionization + capture) processes for protons in water and DNA. The adopted approach will be similar to that reported by Galassi *et al* (2002), where the double ionizing processes were treated within an independent-event model with single particle probabilities calculated as a function of the impact parameter using the CDW-EIS model. Additionally, the double ionization induced by electron impact will be implemented in a near future into the *TILDA-V* database by means of the

perturbative model provided by Oubaziz *et al* (2015) who recently reported on a quantum mechanical approach providing a quantitative description of the electron-induced double ionization process on isolated water molecules for impact energies ranging from the target ionization threshold up to about 10 keV. Finally, the electron tracking will be completed by the elastic scattering description in DNA. The chosen approach will be based on a partial-wave treatment similar to that reported above for water where the interaction potential will account a static potential numerically deduced from the above-cited molecular wave functions as well as exchange and correlation–polarization contributions. Developments are actually in progress and a forthcoming study will be submitted very soon.

In this context, the *standard* version of *TILDA-V* is based on: *i)* CDW-EIS calculations for describing all the ionizing processes induced by both proton and neutral-hydrogen, *ii)* the semi-empirical approach proposed by Miller and Green (1973) for treating the proton-induced excitation and *iii)* the extrapolation suggested by Uehara *et al* (2000) for describing the neutral-hydrogen induced excitation and electron loss processes (see Table 7).

Location of Table 7

Table 7. List of the theoretical and semi-empirical models currently in use in the *standard* version of *TILDA-V*.

4.1. Proton transport in water: macroscopic outcomes

We first report in Fig.23a the electronic stopping power for protons in water as provided by the *standard* version of *TILDA-V*. To do that, we simulated one million histories of *stationary* protons along which we scored all the inelastic events induced by the primary particle. The stopping power - expressed in keV/μm – is defined as the ratio of the total amount of energy released by the heavy charged particle over the length of the full track. However, for comparison purposes, the *TILDA-V* predictions were normalized per *mass unit* by using the liquid water density ρ = 1g.cm^{-3} and then expressed in MeV.cm^2.g^{-1}. It is worth noting that all the biomolecular targets considered in the current work are treated as isolated molecules (water as well as DNA components). However, it is relevant to assess to which extent the obtained stopping power of protons would differ from gaseous to liquid water. Therefore, we used the same theoretical formalism for both phases in considering nevertheless the “correct” binding energies of the water molecule in the medium considered, arguing that the modification of the water target wave function from vapor to liquid state has only a low impact on the total cross section calculation, as demonstrated by many authors (see for example Champion (2010) who reported a detailed analysis of the electron-induced ionization in gaseous and liquid water). We report hereunder the binding energies of the molecular subshells considered in the description of the water molecule in vapor and liquid state.

Location of Table 8

Table 8. Binding energies (in eV) for the different molecular subshells of the water molecule in gaseous and liquid phases.

Fig.23 compares the stopping power for protons in both phases of water (*TILDA-V*$_{vapor}$ and *TILDA-V*$_{liquid}$, respectively) with the *vapor* stopping cross sections of Reynolds *et al* (1953) (squares) measured over the energy range 30-600 keV, the experimental values of energy loss reported by Phillips (1953) (up-triangles) in the region from 10 to 80 keV, the stopping cross sections of Mitterschiffthaler and Bauer (1990) (circles) in the energy range 25-350 keV, the experimental values of Baek *et al* (2006) (diamonds) in the energy range 1-100 keV and the recent measurements in *liquid* water provided by Shimizu *et al* (2009) (solid up-triangles) for 1-2MeV as well as those reported by Siiskonen *et al* (2011) (solid down-triangles) in the energy range 4.7-15.2 MeV. From a general point of view, we observe that the *TILDA-V*$_{vapor}$ predictions exhibit an excellent agreement with all the *vapor* data available in the literature, except maybe in the very low-energy domain ($E_{inc} < 20$ keV) where the current results slightly underestimate the experiment (≈12-15%). This discrepancy is undoubtedly linked to the current CDW-EIS underestimation of the total ionization cross section in the low-energy range, as reported in Figure 7. Besides, let us remind that in the *TILDA-V* simulations, the protons are followed until their energies become lower than a predefined cut-off of 10 keV. Thus, under "*realistic*" tracking conditions (tracking until the particles stop in matter), the stopping cross sections would be slightly increased. For increasing impact energies, the energy cut-off has a lesser influence and the agreement with the experiment becomes excellent. The maximum experimentally observed appears well reproduced by our calculations, both in shape and magnitude with in particular a location at about $E_{inc} \approx 75$ keV and an amplitude of about 960 MeV.cm^2.g^{-1}.

In *liquid* water, the *TILDA-Vliquid* calculations exhibit stopping power values slightly lower than their *vapor* homologous (≈3-6%), as expected due to the difference of binding energies between the two water phases. The maximum appears at the same proton energy with nevertheless an amplitude slightly lower than the *vapor* corresponding one, namely, of the order of 960 MeV.cm^2.g^{-1}. Excellent agreement is observed between our results and the sole available measurements reported by Shimizu *et al* (1-2MeV) and by Siiskonen *et al* (4.7-15.2 MeV). Nevertheless, let us mention that Shimizu and co-workers' results appear slightly lower than our results, as also mentioned by the authors who underlined a considerable underestimation of about 11% for their results in comparison to the existing standard stopping power data.

Finally, in the inset of Fig.23 that refers to the stopping power of protons in water (the latter being described by its vapor state wave function) we distinguished the proton contribution from the neutral hydrogen one in order to clearly highlight the role played by each projectile type in the particle slowing down in the water medium. From a general point of view, we observe that the hydrogen contribution dominates the energy transfers in the very low-energy regime, namely, below around 30 keV. Beyond this value, the proton contribution becomes dominant, which is obviously related to the fact that at these impact energies, the initial projectile charge ($Z = 1$) remains unchanged *i.e.* equal to 1, the proton-induced electron capture being quasi negligible.

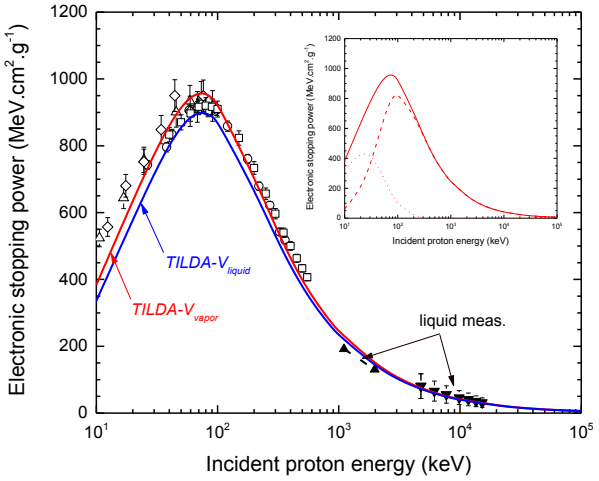

Figure 23. Electronic stopping power as provided by the *standard* version of *TILDA-V* in *liquid* water (*TILDA-V*$_{liquid}$, blue line) as well as in water *vapor* (*TILDA-V*$_{vapor}$, red line). Experimental data are taken from various sources and include measurements in water *vapor* (circles: Mitterschiffthaler and Bauer (1990), up-triangles: Phillips (1953), diamonds: Baek *et al* (2006), squares: Reynolds *et* al (1953)) as well as the recent measurements in *liquid* water provided by Shimizu *et al* (2009) (solid up-triangles) and by Siiskonen *et al* (2011) (solid down-triangles). Inset: total stopping power in water *vapor* (red solid line), H^+ contribution (red dashed line), H^0 contribution (red dotted line) as provided by *TILDA-V*$_{vapor}$.

In Fig.24, the *TILDA-V*$_{vapor}$ and *TILDA-V*$_{liquid}$ predictions are compared with a large series of theoretical/semi-empirical calculations as well as Monte Carlo simulations taken from the literature. As expected, the divergences between the various models essentially appear for impact proton energies lower than about 1 MeV. Thus, Fig.24a and 24b report stopping power results in *vapor* and *liquid* water, respectively, for proton energies limited to the 10 keV-1 MeV range. On the left panel, we first note a very good agreement (< 5%) between our *TILDA-V*$_{vapor}$ results (red line) and the ICRU49 (stars) as well as the SRIM2006 results (dark yellow line) over the whole energy range, with in particular a maximum stopping power of about 930 MeV.cm^2.g^{-1} at $E_{inc} \approx 80$ keV for ICRU49 and of about 916 MeV.cm^2.g^{-1} at $E_{inc} \approx 80$ keV for SRIM2006. With regard to the Janni's tabulation (solid circles), we observe that they are slightly higher than both our results and the ICRU49 and the SRIM2006 data in particular for proton energies lower than 100 keV, the disagreement being more important as the proton energy decreases. The calculations provided by Uehara *et al* (orange line) exhibit very large discrepancies over the whole energy range, with in particular an overestimated maximum value of about 1130 MeV.cm^2.g^{-1} located at lower proton energy ($E_{inc} \approx$ 60-70 keV). Let us mention that Uehara and co-workers' calculations of electronic stopping cross sections are based on a compilation of both experimental and semi-empirical cross sections for describing the main processes induced by protons and hydrogen in water. Furthermore, contrary to our approach Uehara *et al* calculated the energy transfer during the ionization process by simply accounting for average quantities for both the secondary electron energy and the potential energy locally deposited. Similarly, the calculations of Xu *et al* (pink line) performed within a modified local-plasma model largely underestimate the present calculations and surprisingly suggest a maximum located at very low proton energy. Additionally, we

reported the theoretical calculations provided by Fainstein *et al* within the CDW-EIS framework. Evident differences may be observed with our calculations in particular for incident energies lower than 1 MeV. The latter may originate from various sources, including the water target description, which is - in Fainstein and coworkers' work - simply represented as a linear combination of atoms or atomic orbitals (Bragg's additivity rule and CNDO, respectively), whereas a molecular approach was privileged in our work. However, such refinements have been pointed out to have only a low influence, in particular at the single differential scale and obviously more evidently at the total scale. For more details we refer the reader to our recent work (Champion *et al* 2012c) where we analyzed the influence of the molecular target representation in the description of the proton-induced ionization and electron capture by testing three approaches, namely, the well-known Bragg's additivity rule which consists in representing the molecular cross sections as a weighted sum of the cross sections of the different atomic components of the molecule, the complete neglect of differential overlap (CNDO) approach, where the molecular orbitals are expressed in terms of atomic orbitals of the atomic constituents, and finally the MO-LCAO-SCF approach (as provided by Moccia (1964)), which describes the populations of the target by means of molecular orbitals constructed from a linear combination of atomic orbitals in a self-consistent field approximation. In fact, the underestimation observed between the CDW-EIS results of Fainstein *et al.* and our current data essentially comes from the fact that in their work, the authors limited their study to the target ionization/excitation and did not consider the projectile ionization (*i.e.* electron loss process), whose contribution may be important in particular in the energy range investigated here (E_{inc} < 1 MeV). On the right panel, dispersions (< 10%) are also noticeable between our *TILDA-V*$_{liquid}$ (blue line) and the available data. More precisely, we observe a close agreement between the calculations provided by Dingfelder *et al* (2000) (magenta line) and by Date *et al* (2006) (gray line) both based on analytical expression for modeling the proton- and hydrogen-induced interactions as well as with the GEANT4-DNA (orange line) and FLUKA (cyan line) Monte Carlo simulations. The ICRU49 standard data for liquid water (open stars) are also in good agreement. In parallel, the electric-response model of Emfietzoglou *et al* (dark yellow line) exhibits large discrepancies with in particular an abrupt decrease for incident energies lower than about 85-90 keV similarly to the data provided by Xu *et al* (pink line) within a modified local-plasma model which largely underestimate the data reported in the figure.

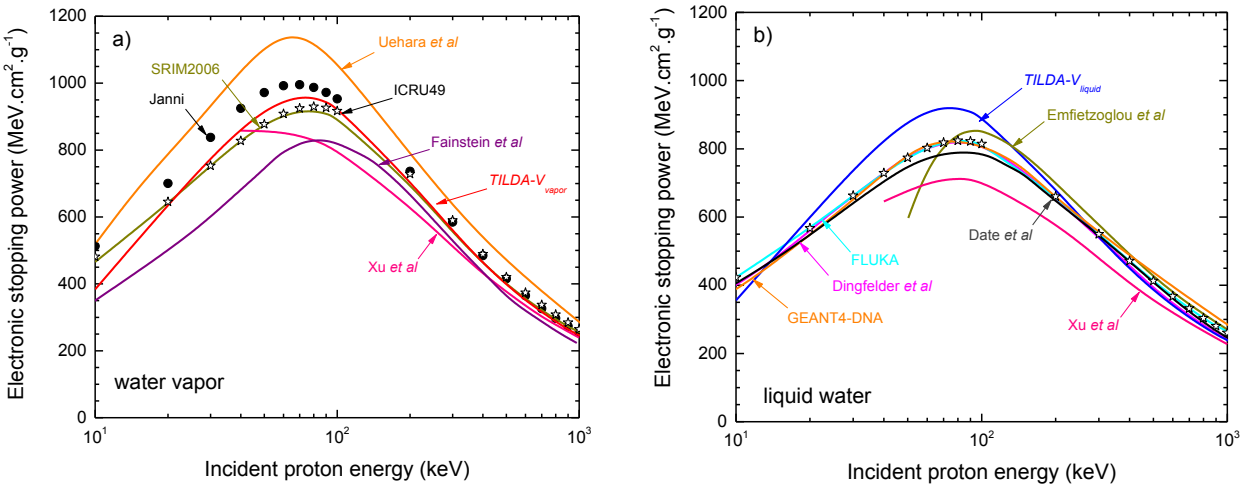

Figure 24. Comparison of our calculations with theoretical data taken from the literature: a) for *vapor*: *TILDA-V*$_{vapor}$ (red line), Uehara *et al* (2001) (orange line), SRIM2006 (Ziegler *et al* (2003)) (dark yellow line), Xu *et al* (1985) (pink line), Fainstein *et al* (1996) (purple line), Janni's tabulation (1982) (circles) and ICRU49 (open stars); b) for *liquid*: *TILDA-V*$_{liquid}$ (blue line), Dingfelder *et al* (2000) (magenta line), FLUKA (private communication) (cyan line), GEANT4-DNA (Incerti *et al* 2010a) (orange line), Date *et al* (2006) (gray line), Emfietzoglou *et al* 2006 (dark yellow line), Xu *et al* (1985) (pink line) and ICRU49 (open stars).

In Fig.25, we compare the proton range in *liquid* water as simulated by the *standard* version of *TILDA-V*$_{vapor}$ and *TILDA-V*$_{liquid}$. The latter was calculated by following one million of proton histories until the primary particle energy is below a predefined energy cut-off, here fixed at 10 keV. The comparison with existing data, namely, Janni's, the ICRU49 and the SRIM2006 tabulations (circles, diamonds and green line, respectively), as well as with the calculations of Uehara *et al* (purple line) and the FLUKA Monte Carlo simulation (cyan line) shows very good agreement along the whole energy range. With regard to the GEANT4-DNA Monte Carlo code (orange line), we observe that the predictions exhibit an overestimation of the proton range for impact energies lower than ≈ 100 keV.

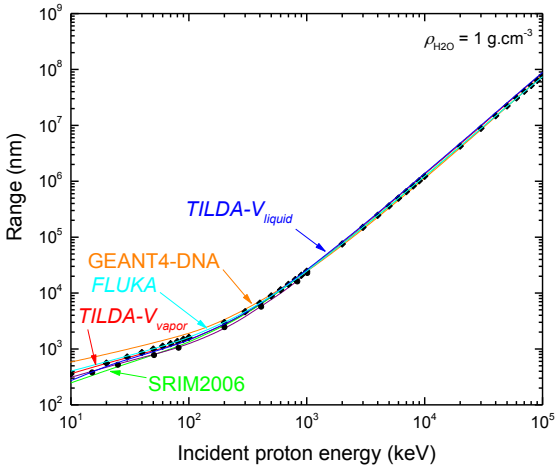

Figure 25. Proton range in *liquid* water as simulated by the *standard* version of *TILDA-V* in *liquid* water (*TILDA-V*$_{liquid}$, blue line) as well as in water vapor (*TILDA-V*$_{vapor}$, red line) compared with available data: Janni's tabulation (1982) (circles), ICRU 49 (1993) (diamonds), Uehara *et al* (2001) (purple line), SRIM2006 (Ziegler *et al* (2003)) (green line), GEANT4-DNA (Incerti *et al* (2010b)) (orange line).

4.2. Influence of the theoretical support in the proton track modeling

In order to estimate the influence of the various theoretical treatments proposed in *TILDA-V* for modeling the proton transport in water, we hereafter calculate the electronic stopping power of protons in water in varying successively the theoretical treatment of: *i)* the proton-induced ionization (Fig.26a), *ii)* the proton-induced electron capture (Fig.26b) and *iii)* the hydrogen-induced ionization (Fig.26c) in keeping - in each case - the *standard* models (see Table 7) for treating the other processes.

In Fig.26a we first analyze the influence of the proton-induced ionization treatment by using the various models implemented into *TILDA-V*$_{vapor}$: the perturbative CB1 theory (orange), the *prior* CDW-EIS approach (red) and the semi-empirical models provided by Hansen and Kocbach (blue), Green and McNeal (green)

and Rudd (magenta). Large discrepancies may be observed, both in shape (location of the position ranging from 40 keV to 100 keV) and magnitude (deviation of about 20%). Indeed, we found that according to the model used for describing the ionization process, large differences might appear whether it is at the total (integrated) scale (see Figure 7) or at the differential level (see for example Champion *et al* 2008). As a consequence, the stopping power reported in Fig.26 exhibits a strong dependency versus the ionization model with in particular an evident correlation with the total ionization cross sections reported in Fig.7. On the contrary, the proton-induced electron capture process exhibits a less pronounced influence on the stopping power calculation (see Fig.26b), except when the CDW model is used (blue line), the latter overestimating the electron capture probability in the low-energy domain (as reported in Fig.11). Finally, Fig.26c shows that the influence of the hydrogen-induced ionization treatment is negligible.

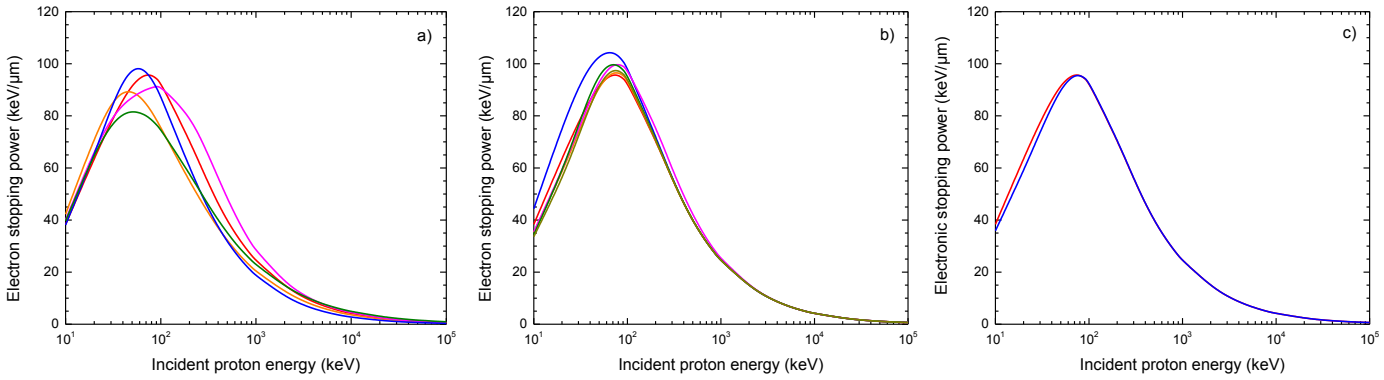

Figure 26. Influence of the main ionizing processes treatment on the electronic stopping power obtained with *TILDA-V*$_{vapor}$. a) Various models for the proton-induced ionization treatment: CB1 (orange), prior CDW-EIS (red), HKS (blue), Green and McNeal (green) and Rudd (magenta), b) Various models for the proton-induced electron capture treatment: CDW-EIS (red), CDW (blue), Green and McNeal (green), Dingfelder (orange), Rudd (magenta) and Miller and Green (dark yellow), c) Various models for the hydrogen-induced ionization treatment: Green and McNeal (blue) and *prior* CDW-EIS (red).

Similarly, the proton range calculation appears as slightly dependent of the theoretical treatments, in particular regarding the ionization description as highlighted in Fig.27a where CB1 (orange), prior CDW-EIS (red), HKS (blue), Green and McNeal (green) and Rudd (magenta) models are successively used for modeling the ionization process in the proton slowing-down in water, the other mechanisms being described by the *standard* models. From a general point of view, all the models give similar tendencies except for the HKS model, which overestimates the range predictions, in particular at high impact energies. Finally, as expected, the electron capture process seems to be weakly influent in the proton range modeling (cf Fig.27b).

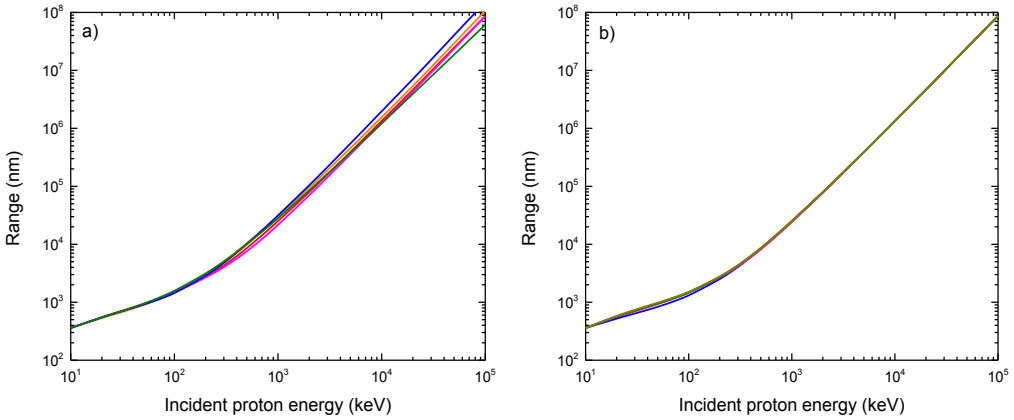

Figure 27. Influence of the proton-induced processes treatment on the range calculations with *TILDA-V*$_{vapor}$. a) Various models for the proton-induced *ionization* treatment: CB1 (orange), prior CDW-EIS (red), HKS (blue), Green and McNeal (green) and Rudd (magenta), b) Various models for the proton-induced *electron capture* treatment: CDW-EIS (red), CDW (blue), Green and McNeal (green), Dingfelder (orange), Rudd (magenta) and Miller and Green (dark yellow).

4.3. From water to DNA

Details on proton-induced collisions in living matter is of prime importance in many fields of medicine ranging from fundamental studies on DNA damage induction for radiobiology to refinement of treatment planning for better radiotherapy strategies in proton therapy. However, and although the use of (liquid) water as a tissue-equivalent medium is widely accepted in the majority of the existing numerical simulations, it remains an unsolved question whether this is the most relevant medium for radiobiological or radiotherapeutical studies. In this context, we have recently reported a detailed analysis of the proton-induced ionization and electron capture processes in water and DNA (Champion *et al* 2015), which pointed out discrepancies in terms of energy deposits between water and DNA (dry as well as hydrated). More importantly, we have shown that these differences were not in the same ratio as the density of the respective medium crossed by the particles and then clearly demonstrated that a simple procedure of density rescaling was inappropriate to reproduce the underlying physics of cellular irradiations. However, this first work was limited to the proton-induced ionizing processes and we are aiming here at comparing the full proton history provided by our Monte Carlo code in water versus DNA.

We report in Figure 28 a detailed analysis of the energy transfers - kinetics as well as potential - occuring along the proton slowing-down in two different biological media, namely, *liquid* water ($\rho = 1.0$ g.cm^{-3}) and *hydrated* DNA ($\rho = 1.29$ g.cm^{-3}, Birnie *et al* (1973)). Such transfers are both due to proton- and hydrogen-induced interactions and are related to the respective singly differential and total cross sections. All the results were obtained by using the *standard* version of *TILDA-V*$_{vapor}$. Fig.28a exhibits the ejection energy distribution induced in water (blue) *vs* DNA (red) as simulated by *TILDA-V*$_{vapor}$ during the proton and hydrogen ionization processes. Only slight differences may be observed between the different media investigated, except in the very low-energy range where the

water spectrum appears slighlty lower than in DNA. Similarly, the asymptotic ejection energy in DNA is about 3% higher than that calculated in water. With regard to the deposited energy spectrum (Figs.28b and 28c), appreciable differences appear between water in DNA, in particular for the capture process. Such observations were pointed out in our previous work (Champion *et al* 2015) where a detailed analysis of the proton-induced electron capture process highlighted the important role played by the sugar-phosphate backbone in the deposited energy pattern. This specificity is related to the high-magnitude of the molecular binding energies of the subshells involved in the collisions, and more particularly the inner-shells, even considering the Auger cascade decay (as done in our calculations), which slighltly modifies the final energy spectrum.

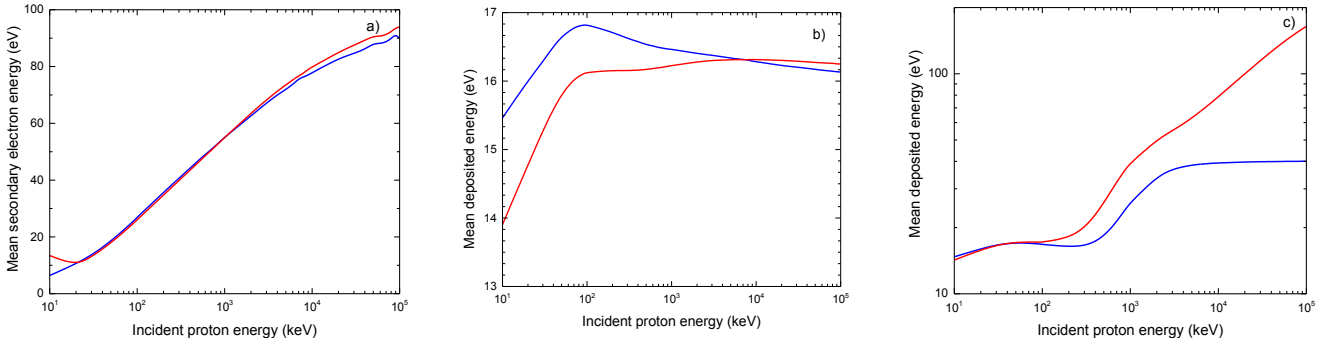

Figure 28. *TILDA-V*$_{vapor}$ simulation of proton track structure in biological matter: water (blue) *vs* DNA (red): a) mean secondary electron energy during the ionization process, b) mean deposed energy during the ionization process, c) mean deposed energy during the capture process.

Finally, Figure 29 exhibits the electronic stopping power for protons in water versus DNA. The results reported in Fig.29a display a very similar behaviour for both media, with in particular a maximum stopping power located at the same proton energy E_{inc} = 70 keV, pointing out nevertheless an overestimation of about 20% in DNA, that clearly reveals that the approach commonly used in many Monte Carlo studies - which consists in rescaling the water vapour based track-structure simulations by a realistic density ρ_{DNA}/ρ_{H2O} - is inappropriate for mimicking the biological reality, in particular at the DNA scale and in cellular environment.

Only few stopping power calculations have been reported in the literature and are - to the best of our knowledge - limited to the calculations of Tan *et al* (2006) and to the recent work of Abril *et al* (2011), which were both performed within the dielectric formalism but with different approaches to evaluate the electron loss function of DNA (in particular in the non-optical limit). Fig.29b shows a comparison of our *TILDA-V*$_{DNA}$ results with these calculations and exhibit very good agreement for $E_{inc} > 100$ keV. For lower energies, Tan *et al's* calculations predict a surprisingly abrupt decrease, while Abril and co-workers' calculations slighlty underestimate our *TILDA-V*$_{DNA}$ calculations by 10-20%.

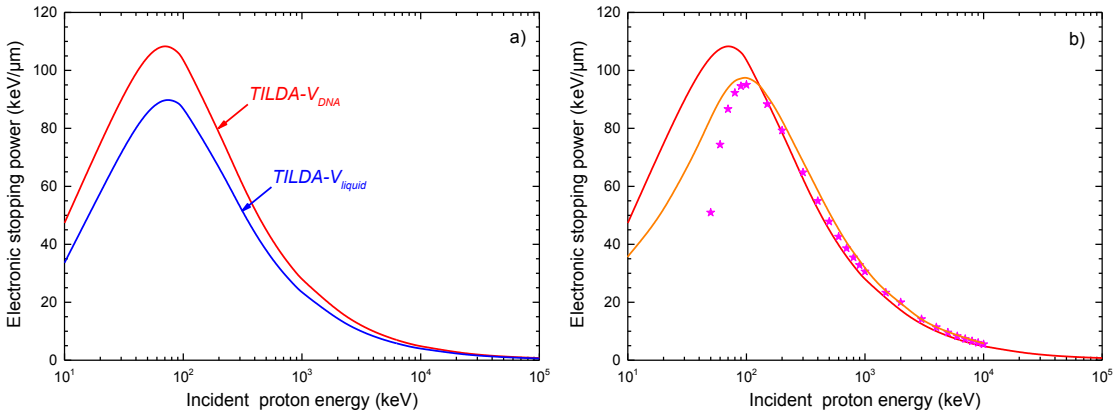

Figure 29. a) Electronic stopping power in water (blue) versus DNA (red) as provided by the *standard* version of *TILDA-V*; b) Stopping power in DNA: comparison of the *TILDA-V*$_{DNA}$ predictions (red line) with existing data: Tan *et al* (2006) (magenta stars) and Abril *et al* (2011) (orange line).

4.4. Dosimetry

Another way to check the reliability of our *TILDA-V* consisted in comparing simulated proton dose profiles to data available in the literature. We followed the procedure proposed by Wiklund *et al* (2008), which consists in subdividing the proton track in cylindrical shells with a logarithm size (33 bins in radial range from 0.1 nm to 240 nm) and scoring all the secondary electron histories along a 40 µm proton track. The results for 1 MeV proton are depicted in Figure 30 along with a selection of Monte Carlo results available in the literature, namely, the LIonTrack simulations (Bäckström *et al* 2013) (dark yellow line), the results provided by Uehera *et al* (2001) (orange line), the GEANT4-DNA predictions (Incerti *et al* 2014) (magenta line), the Olko *et al* results (1989) (purple line) and the data provided by Emfiezoglou *et al* (2004) (violet line). Experimental data taken from Wingate and Baum (1976) (stars) are also reported for comparison. A Very good agreement is observed between our simulation (red line) and Wiklund *et al's* results (green line) even at small radius (< 1 nm), which stems from the fact that the Monte Carlo code developed by these authors is based on a similar CDW-EIS theory than ours for treating the secondary electron emission. Slight differences are nevertheless perceptible, which are undoubtedly due to the variant of secondary particle tracking, which is performed by using the PENELOPE code in the work of Wiklund *et al* (2008). In comparison, the LionTrack profile (blue line) largely underestimates our results as well as the experimental data for $r < 1$ nm, whereas it tends to overestimate the data for higher radii. This disagreement is especially surprising since the CDW-EIS model is here also employed for describing the proton-induced ionization process as well as the PENELOPE code for modeling the secondary electron tracks. However, the authors pointed out that the input dataset used for tracking the secondary electrons in their simulations was Dingfelder's database cross sections (Bäckström *et al* 2013, Dingfelder *et al* 1998, Dingfelder *et al* 2008), whereas the *default* PENELOPE database was used in the work of Wiklund *et al*. Besides, let us note that the profiles provided by Olko *et al* - based on MOCA-8 and MOCA-14 track-structure codes - (purple line) and those reported by Emfiezoglou *et al* (violet line) within the dielectric response model appear as largely overestimating, in particular in the low-radius domain ($r < 1$ nm), while they converge to our results at

higher distances. Finally, the GEANT4-DNA predictions (magenta line) as well as Uehara's Monte Carlo simulations exhibit overall fair agreement, although they used different bin number and radial range.

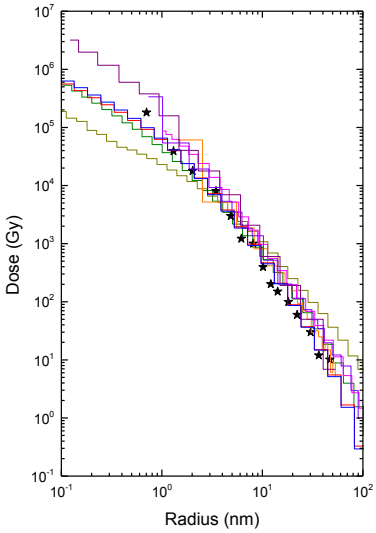

Figure 30. (Color online) Radial dose profile for 1 MeV protons in water. Comparison of *TILDA-V*$_{vapor}$ and *TILDA-V*$_{liquid}$ predictions (red and blue line, respectively) with existing Monte Carlo simulations in water *vapor* (Olko *et al* (1989) (purple line) and Uehara *et al* (2001) (orange line)) and *liquid* water (Wiklund *et al* (2008) (green line), LIonTrack (Bäckström *et al* 2013) (dark yellow line), GEANT4-DNA (Incerti *et al* 2014) (magenta line), Emfietzoglou *et al* (2004) (violet line)). Experimental data are taken from Wingate and Baum (1976) (stars) and refer to measurements in water *vapor*.

In parallel, the literature also reports some *analytical* dose profiles in water. We compare in Figure 31 the radial dose distribution for 1 MeV proton provided by *TILDA-V*$_{vapor}$ with the CDW-EIS calculations provided by Olivera *et al* (magenta line), the semi-analytical results reported by Wilkund *et al* (green line) and the semi-empirical predictions of Butts and Katz (orange line). Very good agreement is observed between our profiles and the experimental vapor data reported by Wingate and Baum (stars) as well as with Olivera and co-workers' calculations. On the contrary, the data reported by Wiklund *et al* (green line) slightly tend to overestimate our calculations at large distances while Butts and Katz predictions (orange line) overestimate all the profiles until 10 nm from the ion track.

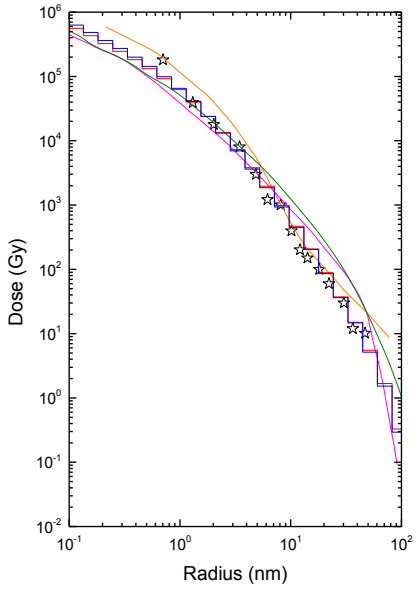

Figure 31. (Color online) Radial dose profile for 1 MeV protons in water. Comparison of the *TILDA-V*$_{vapor}$ and *TILDA-V*$_{liquid}$ results (red and blue line, respectively) with semi-analytical and analytical calculations for water *vapor* (Butts and Katz (1967) (orange line) and Olivera *et al* (1996) (magenta line)) and *liquid* water (Wiklund *et al* (2008) (green line)). Experimental data are taken from Wingate and Baum (1976) (stars) and refer to measurements in water *vapor*.

Apart from the fact that *TILDA-V* is based on a large quantum mechanical input database, it is worth noting that it includes a multi-differential description for all the collisions considered (elastic as well as inelastic) and also access to the full kinematics of the ionization process and more particularly to the angular distribution of the secondary electrons. Indeed, contrary to the major part of existing Monte Carlo codes (FLUKA (private communication) LEPTS (Fuss *et al* (2011)), GEANT4-DNA (Incerti *et al* (2010)), PARTRAC (Friedland *et al* (2003)), Uehara *et al* (2001), Endo *et al* (2002)…) which consider that the secondary electrons are emitted in the momentum transfer direction, *TILDA-V* describes the proton-induced ionization process by means of doubly differential cross sections as it is the case also in a few Monte Carlo codes (Lion Track (Bäckström *et al* (2013) and Wiklund *et al* (2008)). From the theoretical point of view, considering that electrons are emitted in the transfer direction correspond to binary collisions in which the energy lost by the incident particle is completely transferred to the target molecular electron, with the residual ion acting as a spectator. This region, called Bethe ridge, can be simply defined by considering the collision of an incident projectile with a target electron at rest. After the collision, the electron recoils at an angle θ_e with kinetic energy E_e and corresponding momentum $\boldsymbol{k}_e$, while the incident ion is scattered at an angle θ_s with kinetic energy $E_s = E_{inc}–E_e–I_j$ and corresponding momentum $\boldsymbol{k}_s$, where I_j represents the binding energy of the molecular subshell ionized. Thus, from momentum conservation, we obtain $\cos\theta_e^{Bethe} = \dfrac{k_{inc}^2 + k_e^2 - k_s^2}{2k_{inc}k_e}$. However, in Boudrioua *et al* (2007), we have clearly shown that such approximation remains valid provided that the ejected electron energy is high enough since for low ejection

energies the angular distribution becomes more and more isotropic and then far to be peaked in the $\theta_e = \theta_e^{Bethe}$ direction. Let us add that this point is all the more important that the low-energy electrons represent the majority of emitted particles.

Under these conditions, it is important to analyze the impact of the secondary electron angular emission treatment in microdosimetry. Therefore, we have computed dose profiles by considering both the analytically calculated emission angle θ_e^{Bethe} and that deduced from random sampling among doubly differential cross sections. The results are shown in Figure 32 for two different incident proton energies, namely, 100 keV and 1 MeV. In Fig.32a, we observe that the two sets of results agree well provided that $r \geq 1\,\text{nm}$, whereas large discrepancies appear in the close vicinity of the ion track with in particular an underestimation of the order of 200% at $r = 0.1$ nm for the classical description. For higher proton energy (see Fig.32b), the divergences diminish but remain nevertheless noticeable for $r \leq 1\,\text{nm}$. These results undoubtedly demonstrate the absolute necessity of using accurate cross sections in the electron emission description for any study devoted to the proton damage induction modeling at the DNA level. Similar observations were previously reported by Cucinotta *et al* (1995) in a NASA Technical Memorandum, where the authors clearly mentioned that more information on the doubly differential cross sections for electron emission were required in Monte Carlo simulations. Recently, Moribayashi (2015) analyzed in the context of treatment planning in cancer therapy the effect of emission angles of secondary electrons on radial dose profiles and concluded on the crucial importance of the emission angular distribution description.

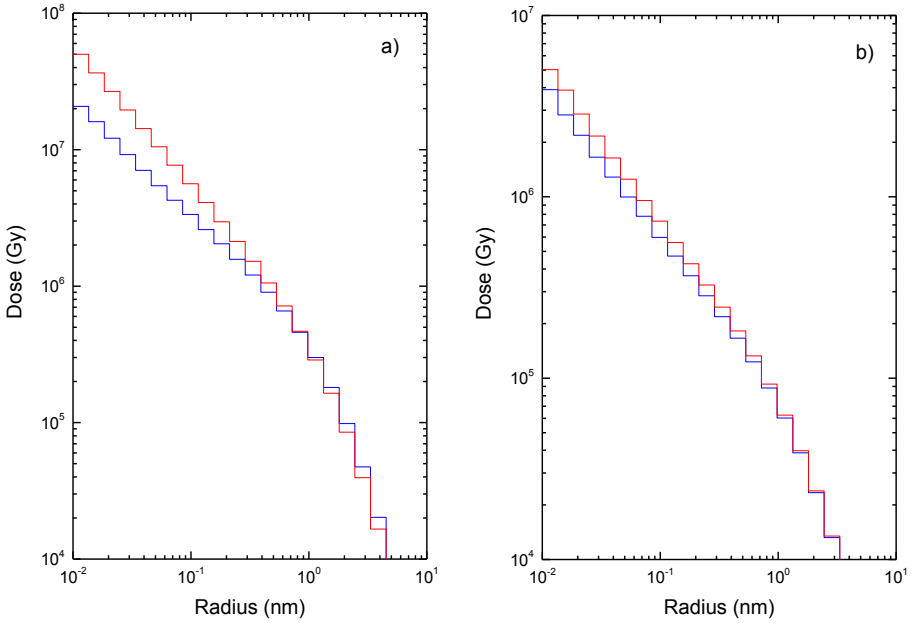

Figure 32. (Color online) Radial dose profiles for 100 keV (panel a) and 1 MeV (panel b) protons in water *vapor* as provided by *TILDA-V*$_{vapor}$: the red line refers to a secondary electron angular distribution sampled from quantum mechanical cross sections whereas the blue line refers to a classical analytical description.

Conclusions

Whether it is for radiotherapy or radioprotection purposes, a fine understanding of the underlying physics of radiations in living matter is an essential prerequisite of any research at the physics and biology frontier. In this context, Monte Carlo simulations are now accepted as the most suitable and powerful tool for investigating the radio-induced interactions. We have here detailed our *TILDA-V* code, which refers to a transport code aiming at describing the track-structure of protons and its secondaries in living matter that includes both water and biological species. All the collisions are described at the nanometric scale by means of a large database including total cross sections as well as a variety of differential cross sections ranging from triply to singly differential ones. All the steps of development were validated by theoretical-experimental confrontations in order to select the most appropriate theories for modeling the proton-, hydrogen- and electron-induced interactions with water and DNA targets both described within a molecular approach. To the best of our knowledge, such a quantum-mechanically based proton transport modeling in a "realistic" biological environment is unique in the dedicated literature.

The present work details the up-to-date version of *TILDA-V* and reviews - interaction by interaction - the implemented quantum components by means of comparisons with existing models. Monte Carlo outcomes including electronic stopping power, range and dose profiles of protons in water and DNA are also provided and compared to available calculations and simulations. The results obtained are finely scrutinized in order to point out the impact of the inelastic interactions modeling on the charged-particle transport in particular when information at DNA level is required.

This well-documented study will serve as a reference work for our forthcoming investigations focused on a water *vs* DNA analysis via Monte Carlo simulations of proton histories in complex environment.

Acknowledgments

We are very grateful to Dr J. E. Groetz (Lab. Chrono Environment, Univ. Besançon, France) for providing us the FLUKA data and his comments about this work. Sandia National Laboratories is a multi-program laboratory managed and operated by Sandia Corporation, a wholly owned subsidiary of Lockheed Martin Corporation, for the U.S. Department of Energy's National Nuclear Security Administration under contract DE-AC04-94AL85000.

References

Abicht F, Prasad R, Borghesi M, Priebe G, Braenzel J, Andreev A, Nickles P V, Schnürer M, Jequier S, Revet G, Tikhonchuk V and Ter-Avetisyan S 2013 Energetic beams of negative and neutral hydrogen from intense laser plasma interaction *Applied Phys. Lett.* **103** 253501

Abril I, Garcia-Molina R, Denton C D, Kyriakou I, and Emfietzoglou D 2011 Energy Loss of Hydrogen- and Helium-Ion Beams in DNA: Calculations Based on a Realistic Energy-Loss Function of the Target *Radiat. Res.* **175** 247-255

Abufager P N, Martínez A E, Rivarola R D and Fainstein P D 2004 CDW-EIS model for single-electron capture in ion–atom collisions involving multielectronic targets *J. Phys. B: At. Mol. Opt. Phys.* **37** 817–827

Agostinelli *et al*. 2003 Geant4-a simulation toolkit *Nucl. Instrum. Methods Phys. Res. A* **506** 250–303

Aouchiche H, Champion C, and Oubaziz D 2008 Electron and positron elastic scattering in gaseous and liquid water: A comparative study *Radiat. Phys. Chem.* **77** 107-114 (2008)

Bäckström G, Galassi M E, Tilly N, Ahnesjö A and Fernández-Varea J M 2013 Track structure of protons and other light ions in water: Application of the LIonTrack code at the nanometer scale *Med. Phys.* **40** 064101

Baek W Y, Grosswendt B, Willems G 2006 Ionization ranges of protons in water vapour in the energy range 1-110 keV *Radiat. Prot. Dosimetry* **122** 32

Bazin M, Michaud M and Sanche L 2010 Absolute cross sections for electronic excitations of cytosine by low energy electron impact *J. Chem. Phys.* **113** 155104

Belkic Dz, Gayet R and Salin A 1979 Electron capture in high-energy ion-atom collisions *Phys. Rep.* **56** 279–369

Berger M J 1993 Report NISTIR-5113 National Institute of Standards and Technology

Bernal M A and Liendo J A 2006 The HKS model for electrons production in liquid water by light ions *Nucl. Instr. Meth. Phys. Res. B* **251** 171–176

Bernal M A, Sikansi D, Cavalcante F, Incerti S, Champion C, Ivanchenko V, and Francis Z 2013 An atomistic geometrical model of the B-DNA configuration for DNA-radiation interaction simulations *Comput. Phys. Comm.* **184** 2840-2847

Bernal M A, de Almeida C E, Incerti S, Champion C, Ivanchenko V, and Francis Z 2015 The influence of DNA configuration on the direct strand break yield *Computational and Mathematical Methods in Medicine*

Bernhardt Ph and Paretzke H G 2003 Calculation of electron impact ionisation cross sections of DNA using the Deutsch-Märk and Binary-Encounter-Bethe formalisms *Int. J. Mass. Spectrom.* **223-224** 599

Birnie G D, Rickwood D, and Hell A 1973 Buoyant densities and hydration of nucleic acids, proteins, and nucleoprotein complexes in Metrizamide *Biochim. Biophys. Acta* **331** 238-294

Bolorizadeh M A and Rudd M E 1986a Angular and energy dependence of cross sections for ejections of lectrons from water vapor. II.15-150-keV proton impact *Phys. Rev. A* **33** 888

Bolorizadeh M A and Rudd M E 1986b Angular and energy dependence of cross sections for ejections of lectrons from water vapor. III.20-150-keV neutral-hydrogen impact *Phys. Rev. A* **33** 893

Boudrioua O, Champion C, Dal Cappello C and Popov Y V 2007 Ab initio calculation of differential and total cross sections for the ionization of water vapor by protons *Phys. Rev. A* **75** 022720

Bremner L J, Curtis M G and Walker I C 1991 Electronic states of some simple ethers studied by vacuum ultraviolet absorption and near-threshold electron energy-loss spectroscopy *J. Chem. Soc. Faraday*

Trans. **87** 1049–1055

Bug M U,2014 University of Wollongong Thesis Collection

Butts J J and Katz R 1967 Theory of RBE for heavy ion bombardment of dry enzymes and virus *Radiat. Res*. **30**, 855–871

Champion C, Hanssen J and Hervieux P A 2002a Theoretical differential and total sections of water-molecule ionization by electrons impact *Phys Rev A* **65** 022710

Champion C, Hanssen J and Hervieux P A 2002b Electron impact ionization of water molecule *J. Chem. Phys*. **117** 197-204

Champion C 2003 Theoretical cross section for electron collision in water: structure of electron tracks *Phys. Med. Biol*. **48** 2147

Champion C, L'Hoir A, Politis M F, Fainstein P D, Rivarola R D and Chetioui A 2005 A Monte Carlo Code fot the Simulation of Heavy-Ion Tracks in Water *Radiat. Res*. **163** 222

Champion C, Dal Cappello C, Houamer S and Mansouri A 2006 Single ionization of the water-molecule by electron impact: angular distributions at low incident energy *Phys. Rev. A* **73** 012717

Champion C, Boudrioua O and Dal Cappello C 2008 Water molecule ionization by charged particles: a short review *J. Phys: Conf. Series* **101** 012010

Champion C, Lekadir H, Galassi M E, Fojón O, Rivarola R D and Hanssen J 2010 Theoretical predictions for ionization cross sections of DNA nucleobases impacted by light ions *Phys. Med. Biol*. **55** 6053

Champion C 2010 Electron impact ionization of liquid and gaseous water: single-center partial-wave approach *Phys. Med. Biol*. **55** 11

Champion C, Le Loirec C, and Stosic B 2012a EPOTRAN: a full-differential Monte Carlo code for electron and positron transport in liquid and gaseous water *Int. J. Radiat. Biol*. **88** 62-65

Champion C, Weck P F, Lekadir H, Galassi M E, Fojón O, Abufager P, Rivarola R D and Hanssen J 2012b Proton-induced single electron capture on DNA/RNA bases *Phys. Med. Biol*. **57** 3039

Champion C, Galassi M E, Weck P F, Fojón O, Hanssen J and Rivarola R D 2012c Quantum-Mechanical Contributions to Numerical Simulations of Charged Particle Transport at the DNA Scale, Springer, Radiation Damage in Biomolecular Systems, Biological and Medical Physics, Biomedical Engineering, G. G. Gómez-Tejedor and M. C. Fuss (eds.), Springer Science, pp. 263-289

Champion C 2013 Quantum-mechanical predictions of electron-induced ionization cross sections of DNA components *J. Chem. Phys*. **138** 184306

Champion C, Hanssen J and Rivarola R D 2013 The first Born approximation for ionization and charge transfer in energetic collision of multiply charged ions with water, *Book Series: Advances in Quantum Chemistry*

Champion C, Galassi M E, Weck P F, Abdallah C, Francis Z, Quinto M A, Fojón O A, Rivarola R D, Hanssen J, Iriki Y and Itoh A 2014 Ionization induced by protons on isolated molecules of adenine: theory, modelling and experiment *J. Phys. Conf. Ser*. **488** 012038

Champion C, Quinto M A, Monti J M, Galassi M E, Weck P F, Fojón O A, Hanssen J and Rivarola R D 2015 Water versus DNA: New insights into proton track-structure modelling in radiobiology and radiotherapy *Phys. Med. Biol*. **60** 7805-7828

Champion C, Monti J M, Quinto M A, and Rivarola R D 2016 Neutral-hydrogen *versus* proton induced ionization in water vapor *Phys. Rev. A* submitted

Champion C and Quinto M A 2016 Elastic scattering of protons in water and DNA: an intra comparison at the differential and integrated scales *Phys. Med. Biol*. submitted

Chatterjee A and Holley W 1993 Computer Simulation of Initial Events in the Biochemical Mechanisms of DNA Damage *Adv. Radiat. Biol*. **17** 181–226

Cheshire I M 1964 Continuum distorted wave approximation: resonant charge transfer by fast protons in atomic hydrogen *Proc. Phys. Soc*. **84** 89–98

Cho H, Park Y S, Anaka H T, Buckman S J 2004 Measurements of elastic electron scattering by water

vapour extended to backward angles *J. Phys. B: At. Mol. Opt. Phys.* **37** 625–634

Cobut V, Cirioni L and Patau J P 2004 Accurate transport simulation of electron tracks in the energy range 1 keV–4 MeV *Nucl. Instrum. Methods B* **215** 57–68

Colson A O, Besler B, and Sevilla M D 1993 Ab initio molecular orbital calculations on DNA radical ions. 3. Ionization potentials and ionization sites in components of the DNA sugar phosphate backbone *J. Phys. Chem.* **97** 8092

Dagnac R, Blanc D, and Molina D D 1970 A study on the collision of hydrogen ions H_1^+, H_2^+ and H_3^+ with a water-vapour target *J. Phys. B* **3** 1239-1251

Danjo A, Nishimura H 1985 Elastic scattering of electrons from H2O molecule *J. Phys. Soc. Jpn.* **54** 1224–1227

Date H, Sutherland K L, Hayashi T, Matsuzaki Y, Kiyanagi Y 2006 Inelastic collision processes of low-energy protons in liquid water *Nucl. Instrum. Methods B* **75** 179–187

Dingfelder M, Hantke D, Inokuti M and Paretzke H G 1998 Electron inelastic-scattering cross sections in liquid water *Radiat. Phys. Chem.* **53** 1–18

Dingfelder M, Inokuti M and Paretzke H G 2000 Inelastic-collision cross sections of liquid water for interactions of energetic protons *Radiat. Phys. Chem.* **59** 255-275

Dingfelder M, Travia A, McLawhorn R A, Shinpaugh J L and Toburen L H 2008 Electron Emission from Foils and Biological Materialsafter Proton Impact *Radiat. Phys. Chem.* **77** 1213-1217

Dingfelder M 2014 Updated model for dielectric response function of liquid water *Applied Radiation and Isotopes* **83** 142-147

Djuric N L, Cadez I M and Kurepa M V 1988 H_2O and D_2O total ionization cross sections by electron impact *Int. J. Mass. Spectrom. Ion. Process.* **83** R7

Douglass M J, Bezak E and Penfold S 2012 Development of a 3D randomised cell death model for Monte Carlo microdosimetry simulations *Med. Phys.* **39** 3509–19

Edel S 2006 PhD Thesis Modélisation du transport des photons et es électrons dans l'ADN plasmide, Université Paul Sabatier, Toulouse

Emfietzoglou D, Karava K, Papamichael G, and Moscovitch M 2003 Monte Carlo simulation of the energy loss of low-energy electrons in liquid water *Phys. Med. Biol.* **48** 2355-2371

Emfietzoglou D, Karava K, Papamichael G and Moscovitch M 2004 Monte Carlo calculations of radial dose profile and restricted LET for proton in water *Radiat. Prot. Dosimetry*, **110**, 871–879

Emfietzoglou D, Pathak A, Papamichael G, Kostarelos K, Dhamodaran S, Sathish N and Moscovitch M 2006 A study on the electronic stopping of protons in soft biological matter *Nucl. Instr. Methods Phys. Res. B* **242** 55-60

Emfietzoglou D, Kyriakou I, Garcia-Molina R, Abril I, and Nikjoo H 2013 Inelastic Cross Sections for Low-Energy Electrons in Liquid Water: Exchange and Correlation Effects *Radiat. Res.* **180** 499-513

Endo S, Yoshida E, Nikjoo H, Hodhi M, Ishikawa M, and Shizuma K 2002 A Monte Czarlo track structure code for low energy protons *Nucl. Instr. Methods Phys. Res. B* **194** 123-131

Fainstein P D, Olivera G H, and Rivarola R D 1996 Theoretical calculations of the stopping power for protons traversing H, He and simple molecular targets *Nucl. Instrum. Methods B* 107 19–26

Fasso A, Ferrari A, Ranft J and Sala P 2005 Current version of FLUKA 2005.6

Fleig T, Kneht S and Hättig C 2007 Quantum-Chemical Investigation of the Structures and Electronic Spectra of the Nucleic Acid Bases at the Coupled Cluster CC2 Level *J. Phys. Chem. A* **111** 5482–5491

Friedland W, Jacob P, Paretzke H. G. and Stork T 1998 Monte Carlo Simulation of the Production of Short DNA Fragments by Low-Linear Energy Transfer Radiation Using Higher-Order DNA Models *Radiat. Res.* **150** 170-182

Friedland W, Jacob P, Bernhardt P, Paretzke H G, Dingfelder M 2003 Simulation of DNA damage after proton irradiation *Radiat. Res* **159** 401–410

Friedland W, Dingfelder M, Kundrát P and Jacob P 2011 Track structures, DNA targets and radiation effects in the biophysical Monte Carlo simulation code PARTRAC *Mutation Res*. **711** 28-40

Frisch M J *et al* 2009, *Gaussian 09*, Revision A.02, Gaussian, Inc., Wallingford CT

Fuss M, Sanz A G, Muñoz A, Blanco F, Téllez M, Huerga C and Garcia G 2011 LEPTS-a radiation-Matter Interaction Model at the Molecular Level and its Use in Biomedical Applications *In* Biomedical Enginnering Trends in Electronics, Communications and Software, Eds. A N Laskovski, Chap. 15, 277-294

Galassi M E, Abufager P N, Martinez A E, Rivarola R D, and Fainstein P D 2002 The continuum distorted wave eikonal initial state model for transfer ionization in H^+, He^{2+}+ He collisions, *J. Phys. B: At. Mol. Opt. Phys*. **35** 1727-1739

Galassi M E, Champion C, Weck P F, Rivarola R D, Fojón O and Hanssen J 2012 Quantum mechanical prediction of DNA and RNA base ionization by energetic proton beams *Phys. Med. Biol*. **57** 2081

Garcia-Molina R, Abril I, Heredia-Avalos S, Kyriakou I, and Emfietzoglou D 2011 A combined molecular dynamics and Monte Carlo simulation of the spatial distribution of energy deposition by proton beams in liquid water *Phys. Med. Biol*. **56** 6475-6493

Gervais B, Beuve M, Olivera G H, Galassi M E, and Rivarola R D 2005 Production of HO_2 and O_2 by multiple ionization in water radiolysis by swift carbon ions *Chem. Phys. Lett*. **410** 330-334

Gobet F, Farizon B, Farizon M and Gaillard M J 2001Total, partial, and electron-capture cross section for ionization of water vapor by 20–150 keVprotons *Phys. Rev. Lett*. **86** 3751

Gobet F, Eden S, Coupier B, Tabet J, Farizon B, Farizon M, Gaillard M J, Ouaskit S, Carre M and Märk T D 2006 Electron-loss and target ionization cross section for water vapor by 20–150 keV neutral atomic hydrogen impact *Chem. Phys. Lett*. **421** 68

Green A E S and Dutta S K 1967 Semi empirical cross sections for electron impact *J. Geophys. Res*. **72** 3933

Green A E S and McNeal R J 1971 Analytic cross section for inelastic collisions of proton and hydrogen atoms with atomic and molecular gases *J. Geophys. Res*. **76** 133

Gudowska I, Sobolevsky N, Andreo P, Belkic D and Brahme A 2004 Ion beam transport in tissue-like media using the Monte Carlo code SHIELD-HIT *Phys. Med. Biol*. **49** 1933-1958

Hamm R N, Ritchie R H, Turner J E, and Wright HA 1982 Inelastic cross sections for electron interactions in liquid water. *In* Workshop on the interface between radiation physics and radiation chemistry. Argonne: Report N°82-88

Hamm R N, Turner J E, Ritchie R H, and Wright H A 1985 Calculation of heavy-ion tracks in liquid water *Radiat. Res*. **104** S20-S26

Hansen J P and Kocbach L 1989 Ejection angle of fast delta electrons from K-shell ionisation induced by energetic ions *J. Phys. B* **22** L71

Hendricks J S, McKinney G.W, Trellue H R, Durkee J W, Roberts T L, Egdorf H W, Finch J P, Fensin M L, James M R. and Pelowitz D B, "MCNPX, Version 2.6. A," Los Alamos National Laboratory Report LA-UR-05-8225 (2005).

Hilgner W, Kessler J, Steeb E 1969 Zur Spinpolarization langsamer Elektronen nach der Streuung an Molekülen II. Wismuttriphenyl und Benzol, Wasser, Tetrachlorkohlenstoff *Z. Phys. Hadrons Nucl*. **221** 324–332

Hush N S and Cheung A S 1975 Ionization potentials and donor properties of nucleic acid bases and related compounds *Chem. Phys. Lett*. **34** 11

Incerti S, Ivanchenko A, Karamitros M, Mantero A, Moretto P, Tran H N, Mascialino B, Champion C, Ivanchenko V N, Bernal M A, Francis Z, Villagrasa C, Baldacchino G, Guèye P, Capra R, Nieminen P and Zacharatou C 2010 Comparison of GEANT4 very low energy cross section models with experimental data in water *Med. Phys*. **37** 4692–4708

Incerti S, Baldacchino G, Bernal M A, Capra R, Champion C, Francis Z, Guèye P, Mantero A, Mascialino

B, Moretto P, Nieminen P, Villagrasa C and Zacharatou C 2010b The Geant4-DNA project *International Journal of Modeling, Simulation and Scientific Computing* 1(2) 157-178

International Commission on Radiation Units and Measurements 1970 ICRU Report 16 ICRU Washington DC, USA

International Commission on Radiation Units and Measurements 1993 ICRU Report 49 ICRU Washington DC, USA

International Atomic Energy Agency 1995 Atomic and Molecular Data for Radiation Therapy and Releted Research IAEA–TECDOC–799 IAEA Vienna

Iriki Y, Kikuchi Y, Imai M, and Itoh A 2011a Absolute doubly differential cross sections for ionization of adenine by 1.0 MeV protons *Phys. Rev. A* **84** 032704

Iriki Y, Kikuchi Y, Imai M, and Itoh A 2011b Proton-impact ionization cross sections of adenine measured at 0.5 and 2.0 MeV by electron spectroscopy *Phys. Rev. A* **84** 052719

Iwase H, Niita K, Nakamura T 2002 Development of general-purpose particle and heavy ion transport Monte Carlo code *J. Nucl. Sci.* **39** 1142-1151

Janni J F 1982 Proton range-energy tables, 1 keV-10 GeV Atomic Data Nuclear tables **27** 147

Johnstone W M, Newell W R 1991 Absolute vibrationally elastic cross sections for electrons scattered from water molecules between 6 eV and 50 eV *J. Phys. B: At. Mol. Opt. Phys.* **24** 3633–3643

Joshipura K N, Gangopadhyay S, Limbachiya C G and Vinodkumar M 2007 Electron impact ionization of water molecules in ice and liquid phases *J. Phys: Conf. Series* **80** 012008

Katase A, Ishibashi K, Matsumoto Y, Sakae T, Maezono S, Murukami E, Atanabe K, Maki H 1986 Elastic scattering of electrons by water molecules over the range 100–1000 eV *J. Phys. B: At. Mol. Phys.* **19** 2715–2734

Kim Y-K and Rudd M E 1994 Binary-encounter-dipole model for electron-impact ionization *Phys. Rev. A* **50** 3954-3967

Kim Y K, Santos J P, and Parente F 2000 Extension of the binary-encounter-dipole model to relativistic incident electrons *Phys. Rev. A* **62** 052710

Krämer M and Kraft G 1994 Calculations of heavy ion track structure *Radiat. Environ. Biophys.* **33** 91–109

Krstic P S and Schultz R R 1998 Elastic and related transport cross sections for collisions among isotopomers of $H^+ + H$, $H^+ + H_2$, $H^+ + He$, $H + H$ and $H + H_2$, Oak Ridge National Laboratory, Oak Ridge, 1998, TN 37831-6372

Lappa A V, Bigildeev E A, Burmistrov D S and Vasilyev O N 1993 "Trion" code for radiation action calculations and its application in microdosimetry and radiobiology *Radiat. Environ. Biophys.* 1993 **32** 1–19La Verne J A and S. M. Pimblott 1995 Electron Energy-Loss Distributions in Solid, Dry DNA *Radiat. Res.* **141** 208

La Verne J A and Pimblott S M 1995 Electron Energy-Loss Distributions in Solid, Dry DNA *Radiat. Res.* **141** 208

Lekadir H, Abbas I, Champion C, and Hanssen J 2009a Total cross sections for ionizing processes induced by proton impact on molecules of biological interest: a Classical Trajectory Monte Carlo approach *Nucl. Instrum. Methods Phys. Res., Sect. B* **267** 1011-1014

Lekadir H, Abbas I, Champion C, Fojón O, Rivarola R and Hanssen J 2009b Single-electron loss cross sections of *DNA* and *RNA* bases impacted by energetic multicharged ions: A classical Monte Carlo approximation *Phys. Rev. A* **79** 062710

Levesque P L, Michaud M, Cho W and Sanche L 2005 Absolute electronic excitation cross sections for low-energy electron (5–12 eV) scattering from condensed thymine *J. Chem. Phys.* **122** 224704

Lindsay, B G Sieglaff D R, Smith K A *et al* 1997 Charge transfer of 0.5-, 1.5-, and 5-keV protons with H_2O: Absolute differential and integral cross sections *Phys. Rev. A* **55** 3945-3946

Linert I, Dampc M, Mielewska B, Zubek M 2012 Cross sections for ionization and ionic fragmentation of pyrimidine molecules by electron collisions *Eur. Phys. J. D* ***66*** 20

Luna H, Barros A L F, Wyer J A, Scully S W J, Lecointre J, Garcia P M Y, Sigaud G M, Santos A C F, Senthil V, Shah M B, Latimer C J and Montenegro E C 2007 Water-molecule dissociation by proton and hydrogen impact *Phys. Rev. A* **75** 042711

Martin C 2003 Modélisation des dommages radioinduits sur l'ADN : prise en compte des radicaux libres et des réparations primaires, PhD thesis, Univertity of Toulouse, France

Medin J and Andreo P 1997 PETRA: a Monte Carlo code for the simulation of proton and electron transport in water Internal Report MSF 1997-1, Karolinska Institutet, Stokholm University

Michaud M, Bazin M and Sanche L 2012 Measurement of inelastic cross sections for low-energy electron scattering from DNA bases *Int. Journal. Radiat. Biol.* **88** 15–21

Miller J H, Green A E S 1973 Proton energy degradation in water vapor *Radiat. Res.* **54** 343–363

Milne-Brownlie D S, Cavanagh S J, Lohmann B, Champion C, Hervieux P A, and Hanssen J 2004 Dynamics in electron impact ionization of H_2O *Phys. Rev. A.* **69** 032701

Miraglia J E, Piacentini R D, Rivarola R D and Salin A 1981 Discussion of electron capture theories for ion-atom collisions at high energies *J Phys. B: At. Mol. Opt. Phys.* **14** L197–L202

Mitterschiffthaler C and Bauer P 1990 Stopping cross section of water vapor for hydorgen ions *Nucl. Instrum. Methods Phys. Res. B* **48** 58

Moccia R 1964 One-center basis set SCF MO's. III. H_2O, H_2S, and HCl *J. Chem. Phys.* **40** 2186

Moribayashi K Simulation study of radial dose due to the irradiation of a swift heavy ion aiming to advance the treatment planning system for heavy particles cancer therapy: The effect of emission angles of secondary electrons 2015 *Nucl. Instrum. Methods Phys. Res., Sect. B* **365** 592-595

Nelson W R, Hirayama H and Rogers D W 1985 The EGS4 code system SLAC-Report-265

Neuefeind J, Benmore C J, Tomberli B, Egelstaff P A 2002 Experimental determination of the electron density of liquid H2O and D2O *J. Phys: Condens. Matter* **14** L429–L433

Nikjoo H, Uehara S, Khvostunov I G, Cucinotta F A, Wilson F A, and Goodhead D T 2000 Monte Carlo track structure for radiation biology and space applications *In* 1st International Workshop on Space Radiation Research and 11th Annual NASA Space Radiation Health Investigators' Workshop, Arona (Italy), May 27-31

Nikjoo H, Uehara S, Emfietzoglou D and Cucinotta F A 2006 Track structure codes in radiation research, *Radiat. Meas.* **41** 1052-1074

Nishimura H, Yano K 1988 Total electron scattering cross sections for Ar, N2, H2O and D2O *J. Phys. Soc. Jpn.* **57** 1951–1956.

Olivera G H, Fainstein P D, Rivarola R D 1996 Contribution from the inner shell of water vapor to dose profiles under proton and alpha particle irradiation *Phys. Med. Biol.* **41** 1633–1647

Olivero J J, Stagat R W and Green A E S 1972 Electron depositon in water vapor, with atmospheric applications *J. Geophys. Res.* **77** 4797–4811

Olko P, Booz J, Paretzke H G and Wilson W E 1989 Energy deposition in nanometer sites based on the track structure calculations *Atomic and Molecular Data for Radiotheraphy*, IAEA, 105–116

Oubaziz D, Quinto M A and Champion C 2015 H_2O double ionization induced by electron impact *Phys. Rev. A* **91** 022703

Ottolenghi A, Merzagora M. and Paretzke H G 1997 DNA complex lesions induced by protons and α-particles: track structure characteristic determining linear energy transfer and particle type dependence *Radiat. Environ. Biophys.* **36** 97–103

Panajotović R, Michaud M and Sanche L 2007 Cross sections for low-energy electron scattering from adenine in the condensed phase *Phys. Chem. Chem. Phys.* **9** 138–148

Perkins S T and Cullen D E 1991 "Tables and Graphs of Atomic Subshell and Relaxation Data Derived from the LLNL Evaluated Atomic Data Library (EADL), Z = 1 - 100" Lawrence Livermore National Laboratory, UCRL-50400, 30

Phillips J A 1953 The energy loss of low energy protons insome gases *Phys Rev* **90** 532

Pimblott S M, LaVerne J A, Mozumder A and Green N J B 1990 Structure of electron tracks in water. 1. Distribution of energy deposition events *J. Phys. Chem.* **94** 488–495

Plante I 2011 A Monte-Carlo step-by-step simulation code of the non-homogeneous chemistry of the radiolysis of water and aqueous solutions. Part I: theoretical framework and implementation *Radiat. Environ. Biophys.* **50** 389-403

Privett A J and Morales J A 2014 Electron nuclear dynamics of proton collisions with DNA/RNA bases at E_{Lab} = 80 keV: A contribution to proton cancer therapy research *Chem. Phys. Lett.* **603** 82-88

Quinto M A, Monti J M, Galassi M E, Weck P F, Fojón O A, Hanssen J, Rivarola R D and Champion C 2015 Proton track structure code in biological matter *J. Phys:. Conf. Ser.* **583** 012049

Reynolds H K , Dunbar D N F, Wenzel W A and Whaling W The stopping cross section of gases for protons, 30–600 keV 1953 *Phys. Rev.* **92** 742

Ritchie R H, Hamm R N, Turner J E and Wright H A 1978 6th Symp. on Microdosimetry (Brussels, Belgium) ed J Booz and H G Ebert (London: Harwood Academic) p 345

Rivarola R D, Galassi M E, Fainstein P D, and Champion C 2013 Computation of distorted wave cross sections for high-energy inelastic collisions of heavy ions with water molecules *Book Series: Advances in Quantum Chemistry*

Rudd M E, DuBois R D, Toburen L H, Ratcliffe C A and Goffe T V 1983 Cross sections for ionization of gases by 5-4000-keV protons and for electron capture by 5-150-keV protons *Phys. Rev. A* **28** 3244-3257

Rudd M E, Goffe T V, DuBois R D, and Toburen L H 1985 Cross sections for ionization of water vapor by 7-4000-keV protons *Phys. Rev. A* **31** 492

Rudd M E 1989 User-friendly model for the energy distribution of electrons from proton or electron collisions, *Nucl. Tracks Radiat. Meas.* **16** 213-218

Salvat F, Fernández-Varea J M and J Sempau 2008 OECD Nuclear Energy Agency, Issy-les-Moulineaux

Salvat F 2013 A generic algorithm for Monte Carlo simulations of proton transport *Nucl. Instrum. Methods B* **316** 144–159

Schutten J, de Heer F J, Moustafa H R, Boerboom A J H and Kistenmaker J 1966 On the electronic energy of a one-electron diatomic molecule near the united atom *J. Chem. Phys.* **44** 3924

Shimizu M, Kaneda M, Hayakawa T, Tsuchida H and Itoh A 2009 Stopping cross sections of liquid water for MeV energy protons *Nucl. Instrum. Methods B* **267** 2667–2670

Shyn TW, Grafe, A 1992 Angular distribution of electrons elastically scattered from water vapour *Phys. Rev. A* **46** 4406–4409

Stolterfoht N, DuBois R D and Rivarola R D 1997 Electron Emission in Heavy Ion– Atom Collisions. Springer, New York, NY, USA

Tabet J, Eden S, Feil S, Adboul-Carime H, Farizon B, Farizon M, Ouaskit S and Märk T D 2010 Absolute total and partial cross sections for ionization of nucleobases by proton impact in the Bragg peak velocity range *Phys. Rev. A* **82** 022703

Tan Z, Xia Y, Zhao M and Liu X 2006 Proton stopping power in a group of bioorganic compounds over the energy range of 0.05–10 MeV *Nucl. Instrum. Methods B* **248** 1–6

Terrissol M and Beaudre B A 1990 Simulation of space and time evolution of radiolytic species induced by electrons in water *Radiat. Prot. Dosim.* **31** 171-175

Terrissol M 1994 Modelling of Radiation Damage by ^{125}I on a Nucleosome *Int. J. Radiat. Biol.* **66**, 447-451

Toburen L H, Nakai M Y, and Langley R A 1968 Measurement of High-Energy Charge-Transfer Cross Sections for Incident Protons and Atomic Hydrogen in Various Gases *Phys. Rev.* **171** 114-122

Toburen L H and Wilson W E 1977 energy and angular distribution of electons ejected from water vapor by 0.3–1.5 MeV protons *J. Chem. Phys.* **66** 5202–5213

Tomita H, Kai M, Kusama T and Ito A 1997 Monte Carlo simulation of physicochemical processes of liquid water radiolysis *Radiat. Environ. Biophys* **36** 105–116

Turner J E, Magee J L, Wright H A, Chatterjee A, Hamm R N and Ritchie RH 1983 Physical and Chemical Development of Electron Tracks in Liquid Water *Radiat. Res.* **96** 437–449

Uehara S, Nikjoo H and Goodhead D T 1993 Cross-sections for water vapour for the Monte Carlo electron track structure code from 10 eV to the MeV region *Phys. Med. Biol.* **38** 1841–1858

Uehara S, Nikjoo H and Goodhead D T 1999 Comparison and Assessment of Electron Cross Sections for Monte Carlo Track Structure Codes *Radiat. Res.* **152** 202–13

Uehara S, Toburen L H, Wilson W E, Goodhead DT and Nikjoo H 2000 Calculations of electronic stopping cross sections for low-energy protons in water *Radiat. Phys. Chem.* **59** 1–11

Uehara S, Toburen L H, Nikjoo H 2001 Development of a Monte Carlo track structure code for low-energy protons in water *Int. J. Radiat. Biol.* **77** 139-154

Uehara S and Nikjoo H 2002 Monte Carlo track structure code for low-energy alpha-particles in water *J. Phys. Chem. B* **106** 11051–11063

de Vera P, Garcia-Molina R, and Abril I 2015 Angular and Energy Distributions of Electrons Produced in Arbitrary Biomaterials by Proton Impact *Phys. Rev. Lett.* **114** 018101

Yokoya A, Cunniffe S M T, and O'Neill P 2002 Effect of Hydration on the Induction of Strand Breaks and Base Lesions in Plasmid DNA Films by γ-Radiation *J. Am. Chem. Soc.* **124** 8859-8866

Wiklund K, Olivera G H, Brahme A and Lind B K 2008 Radial secondary electrons dose profiles and biological effects in light-ion beams on analytical and monte carlo calculations using distorted wave cross sections *Radiat. Res.* **170** 83–92

Wilson W E and Paretzke H G 1981 Calculation of Distributions for Energy Imparted and Ionization by Fast Protons in Nanometer Sites *Radiat. Res.* **87** 521–537

Wilson W E and Nikjoo H 1999 A Monte Carlo code for positive ion track simulation *Radiat. Environ. Biophys.* **38** 97–104

Wingate C L and Baum J 1976 Measured radial distributions of the dose and LET for alpha and proton beams in hydrogen and tissue equivalent gases *Radiat. Res.* **65**, 1–79

Wolff W, Luna H, Sigaud L, Tavares A C, Montenegro E C 2014 Absolute total and partial dissociative cross sections of pyrimidine at electron and proton intermediate impact velocities *J. Chem. Phys.* **140** 064309

Xu Y J, Khandelwal G S, and Wilson J W 1985 Proton stopping cross sections of liquid water *Phys. Rev. A* **32** 629-632

Zaider M, Brenner D J and Wilson W E 1983 The Applications of Track Calculations to Radiobiology I. Monte Carlo Simulation of Proton Tracks *Radiat. Res.* **95** 231–247

Ziegler J F, Biersack J P, Littmark U 2003 The Stopping and Range of Ions in Solids. Pergamon Press, New York http://www.srim.org/

Code	*Incident particles*	*Energy range*	*Medium of interest*	*References*
GEANT4	ions, electrons, positrons, photons	250 eV – GeV	various	Agostinelli *et al* 2003
FLUKA	ions	1 keV – TeV	various	Fasso *et al* 2005
MCNPX	ions, neutrons, electrons, positrons, photons	eV – GeV	various	Hendricks *et al* 2005
PHITS	ions	1 MeV – 200 GeV	various	Iwase *et al* 2002
PTRAN	protons	50 MeV – 250 MeV	various	Berger *et al* 1993
SHIELD-HIT		1 MeV/u – 1 TeV/u		Gudowska *et al* 2004
SRIM		1 keV –2 GeV/u		Ziegler *et al* 2003
Monte Carlo track-structure codes				
Code	***Particles***	***Energy range***	***Medium***	***References***
CPA100	***electrons***	10 eV – 100 eV	water (liq)	Terrissol and Beaudre 1990
DELTA	protons, α particles	0.3 eV – 4 MeV/u	water (liq, vap)	Zaider *et al* 1983
	electrons	10 eV – 10 keV		
EPOTRAN	electrons, positrons	7.4 eV – 10 keV	water (liq, vap)	Champion *et al* 2012a
LEPHIST (KURBUC)	protons	1 keV – 1 MeV	water (liq)	Uehara *et al* 1993
	electrons	10 eV – 10 MeV		
LEAHIST (KURBUC)	α particles	1 keV – 2 MeV/u	water (liq)	Uehara and Nikjoo 2002 Uehara *et al* 1993
	electrons	10 eV – 10 MeV		
LIonTrack	ions	1 – 300 MeV/u	water (liq)	Bäckström *et al* 2013
GEANT4-DNA	ions	1 keV – 400 MeV/u	water (liq)	Incerti *et al* 2010a
	electrons	7.4 eV – 1 MeV		
Kramer & Kraft	ions	20 keV – 100 MeV/u	water (liq)	Krämer and Kraft 1994
MC4	ions	> 0.3 MeV/u	water (liq, vap)	Emfietzoglou *et al* 2003
	electrons	> 10 eV		
MOCA14	proton, α particles	0.3 eV – 4 MeV/u	water (vap)	Wilson and Paretzke 1981
MOCA15	proton, α particles	0.3 eV – 4 MeV/u	water (vap)	Ottolenghi *et al* 1997
NOTRE DAME	ions	> 0.3 MeV/u	water (liq, vap)	Pimblot *et al* 1990
	electrons	> 10 eV		
OREC	proton, α particles	0.3 eV – 4 MeV/u	water (liq)	Turner *et al* 1983
	electrons	10 eV – 1 MeV		
PARTRAC	proton, α particles	0.3 eV – 1 GeV/u	water (liq, vap)	Dingfelder *et al* 2000
	electrons	8.23 eV – 10 MeV/u		
PENELOPE	proton	10 keV – 10 GeV	various	Salvat 2013
	electrons, positrons	100 eV – 10 GeV		
PETRA	proton	50 MeV – 250 MeV	various	Medin and Andreo 1997
PITS	ions	0.3 eV – GeV/u	biological	Wilson and Nikjoo 1999
	electrons	> 10 eV		
SHERBROOKE	ions	> 0.3MeV/u	water (liq, vap)	Cobut *et al* 2004
	electrons	> 10 eV		
STBRGEN	ions	0.3 eV – GeV/u	water (liq, vap)	Chatterjee and Holley 1993
	electrons	0.1 – 2 keV		
TILDA	ions	10 keV – 100 MeV/u	water (liq, vap)	Champion *et al* 2005
TRION	ions	> 0.3 MeV/u	water (liq, vap)	Lappa *et al* 1993
	electrons	> 10 eV		

TRACEL	ions	> 0.3MeV/u	water (liq, vap)	Tomita *et al* 1997	
	electrons	> 10 eV			

Table 1. Monte Carlo codes available in the literature

Water				
Shell	***Shell index***	***Subshell***	***Probability***	***Energy (eV)***
$(1a_1)^2$ $(2a_1)^2$ $(1b_2)^2$ $(3a_1)^2$ $(1b_1)^2$	1 2 3 4 5	122	0.0994	478.82
		123	0.0994	493.86
		124	0.1988	493.90
		125	0.1988	493.90
		133	0.1988	508.90
		134	0.1988	508.90
		135	0.1988	508.94
		144	0.1988	508.94
		145	0.1988	508.98
		155	0.1988	508.98
Atomic components of the various biomolecules included in the DNA description				
Carbon				
Subshells			***Probability***	***Energy (eV)***
K	L1	L1	4.13609E-01	255.890
K	L1	L2	1.36190E-01	264.460
K	L1	L3	2.71099E-01	264.470
K	L2	L2	4.20748E-03	273.030
K	L2	L3	1.10012E-01	273.040
K	L3	L3	6.32008E-02	273.050
Nitrogen				
Subshells			***Probability***	***Energy (eV)***
K	L1	L1	2.65388E-01	358.650
K	L1	L2	1.29999E-01	370.250
K	L1	L3	2.58276E-01	370.270
K	L2	L2	8.15943E-03	381.850
K	L2	L3	2.12711E-01	381.870
K	L3	L3	1.22190E-01	381.890
Oxygen				
Subshells			***Probability***	***Energy (eV)***
K	L1	L1	1.78644E-01	478.820
K	L1	L2	1.16224E-01	493.860
K	L1	L3	2.30418E-01	493.900
K	L2	L2	1.10822E-02	508.900
K	L2	L3	2.91115E-01	508.940
K	L3	L3	1.66809E-01	508.980
Phosphorus				
Subshells			***Probability***	***Energy (eV)***
K	L1	L1	7.12845E-02	1756.10
K	L1	L2	7.70090E-02	1804.11
K	L1	L3	1.49534E-01	1805.07
K	L1	M1	1.42971E-02	1926.04
K	L1	M2	3.09277E-03	1934.87
K	L1	M3	6.00170E-03	1934.92
K	L2	L2	1.35789E-02	1852.12
K	L2	L3	3.44468E-01	1853.08
K	L2	M1	6.87552E-03	1974.05
K	L2	M2	1.05204E-03	1982.88
K	L2	M3	1.25152E-02	1982.93
K	L3	L3	1.96055E-01	1854.04
K	L3	M1	1.33713E-02	1975.01
K	L3	M2	1.25043E-02	1983.84

K	L3	M3	1.43892E-02	1983.89
K	M1	M1	7.12833E-04	2095.98
K	M1	M2	2.75938E-04	2104.81
K	M1	M3	5.34626E-04	2104.86
K	M2	M2	1.72459E-05	2113.64
K	M2	M3	3.67923E-04	2113.69
K	M3	M3	2.12700E-04	2113.74
L1 (2s)	L2	M1	2.31157E-01	30.8000
L1 (2s)	L2	M2	4.82015E-02	39.6300
L1 (2s)	L2	M3	4.87713E-02	39.6800
L1 (2s)	L3	M1	4.55856E-01	31.7600
L1 (2s)	L3	M2	4.78317E-02	40.5900
L1 (2s)	L3	M3	1.37702E-01	40.6400
L1 (2s)	M1	M1	9.19772E-03	152.730
L1 (2s)	M1	M2	6.89081E-03	161.560
L1 (2s)	M1	M3	1.36935E-02	161.610
L1 (2s)	M2	M2	8.43928E-05	170.390
L1 (2s)	M2	M3	2.67913E-06	170.440
L1 (2s)	M3	M3	1.74150E-04	170.490
L2 (2p)	M1	M1	3.84224E-02	104.720
L2 (2p)	M1	M2	4.09857E-01	113.550
L2 (2p)	M1	M3	2.66610E-02	113.600
L2 (2p)	M2	M2	1.11541E-01	122.380
L2 (2p)	M2	M3	4.01870E-01	122.430
L2 (2p)	M3	M3	1.15410E-02	122.480
L3 (2p)	M1	M1	3.74626E-02	103.760
L3 (2p)	M1	M2	1.31656E-02	112.590
L3 (2p)	M1	M3	4.23652E-01	112.640
L3 (2p)	M2	M2	1.74570E-03	121.420
L3 (2p)	M2	M3	2.10574E-01	121.470
L3 (2p)	M3	M3	3.13300E-01	121.520

Table 2. Probabilities and corresponding energy transfers for the non-radiative transitions taken into account in *TILDA-V* for water and DNA.

		Semi-empirical models	***Theoretical models***	***Semi-empirical models***	***Theoretical models***
Proton	***Ionization***	Rudd (1989) HKS (Bernal and Liendo 2006) Rutherford (Stolterfoht *et al* 1997)	*prior* CDW-EIS (Rivarola *et al* 2013) CB1 (Boudrioua *et al* 2007) (Champion *et al* 2013)	Rudd (1989) HKS (Bernal and Liendo 2006) Rutherford (Stolterfoht *et al* 1997) see (Champion *et al* 2014) for a comparison	*prior* CDW-EIS (Monti *et al*. 2015) CB1 (Champion *et al* 2010)
	Capture	Rudd (1989) Dingfelder (Dingfelder *et al* 2000) Green and McNeal (1971)	CDW-EIS (*prior*) CDW (Champion *et al* 2012b)		CDW-EIS (*prior*) CDW (Champion *et al* 2012b)
	Excitation	Miller and Green (1973) Dingfelder *et al* (2000)		*home-made* extrapolations	
	Elastic scattering		Classical description (Champion and Quinto 2016)		Classical description (Champion and Quinto 2016)
Neutral hydrogen atom	***Ionization***	Green and McNeal (1971)	*prior* CDW-EIS CBA (Champion *et al*. 2016)		*prior* CDW-EIS CBA (Champion *et al*. 2016)
	Capture	neglected			
	Excitation	Uehara *et al* (2000)		*home-made* extrapolations	
	Electron loss	Dingfelder (Dingfelder *et al* 2000) Green and McNeal (1971)	(*prior*) CDW-EIS (Monti *et al* 2014)		in progress
	Elastic scattering		Classical description of proton (Champion and Quinto 2016) extrapolated to hydrogen as suggested by Endo *et al* (2002)		Classical description of proton (Champion and Quinto 2016) extrapolated to hydrogen as suggested by Endo *et al* (2002)
Electron	***Ionization***	BEB (Kim and Rudd 1994)	DWBA (Champion *et al* 2002a, 2006) (Champion 2010)	BEB (Champion 2013)	CBA (Champion 2013)
	Excitation	Olivero (Olivero *et al* 1972)			*home-made* extrapolations
	Elastic scattering		Partial wave expansion (Champion 2003) (Aouchiche *et al* 2008)		in progress

Table 3. List of the physical models available in *TILDA-V*

	α	β	Ω	$\widetilde{K}$
Adenine	3.8	2	0.7236	206.2
Cytosine	3.8	2	0.7236	170.8
Guanine	3.8	2	0.7236	229.8
Thymine	3.8	2	0.7236	194.4
Sugar Phosphate	3.8	2	0.7236	282.8

Table 4. Fitting parameters for the total cross sections of proton-induced excitation of DNA.

	α	β	Ω	$\widetilde{K}$
Adenine	3.8	2	0.7236	206.2
Cytosine	3.8	2	0.7236	170.8
Guanine	3.8	2	0.7236	229.8
Thymine	3.8	2	0.7236	194.4
Sugar Phosphate	3.8	2	0.7236	282.8

Table 5: Parameters used for the hydrogen-induced excitation in DNA.

	Theory	Experiment
Adenine	5.45	5.8
Cytosine	5.29	5.39
Guanine	5.38	-
Thymine	5.74	5.5
Tetrahydrofuran		7.56

Table 6. Mean excitation energies (in eV) used in *TILDA-V*.

	Process	Model
Proton	Ionization	*prior* CDW-EIS
	Capture	*prior* CDW-EIS
	Excitation	Miller and Green (1973)
	Elastic scattering	Classical description
Hydrogen	Ionization	*prior* CDW-EIS
	Excitation	Uehara *et al* (2000)
	Electron loss	Miller and Green (1973)
	Elastic scattering	Classical description

Table 7. List of the theoretical and semi-empirical models currently in use in the *standard* version of *TILDA-V*.

Water phase	$1b_1$	$3a_1$	$1b_2$	$2a_1$	$1a_1$
Vapor	12.61	14.73	18.55	32.20	539.70
Liquid	10.79	13.39	16.05	32.30	5390.00

Table 8. Binding energies (in eV) for the different molecular subshells of the water molecule in gaseous and liquid phases (Champion *et al* 2012c).